INTELLIGENT SELECTION OF TRANSMISSION WAVEFORM FOR ACTIVE SONAR

USING PREDICTED TARGET STATE

by

Venkata Sasikiran Veeramachaneni
A Thesis
Submitted to the
Graduate Faculty
of
George Mason University
In Partial fulfillment of
The Requirements for the Degree
of
Master of Science
Electrical Engineering

Committee:

_____   Dr. Jill K. Nelson, Thesis Director

_____   Dr. Kathleen E. Wage, Committee Member

_____   Dr. Feitian Zhang, Committee Member

_____   Dr. Monson H. Hayes, Chair, Department
                                  of Electrical and Computer Engineering

_____   Dr. Kenneth S. Ball, Dean, Volgenau
                                  School of Engineering

Date: _____   Fall Semester 2019
                                  George Mason University
                                  Fairfax, VA

Intelligent Selection of Transmission Waveform for Active Sonar using Predicted Target
State

A thesis submitted in partial fulfillment of the requirements for the degree of
Master of Science at George Mason University

By

Venkata Sasikiran Veeramachaneni
Bachelor of Technology
Jawaharlal Nehru Technological University Kakinada, 2014

Director: Dr. Jill K. Nelson, Professor
Department of Electrical and Computer Engineering

Fall Semester 2019
George Mason University
Fairfax, VA

Dedication

I dedicate this thesis to my motherland incredible India and my mother Padmavathi

Acknowledgments

I would like to thank the following people who made this possible ...

Table of Contents

List of Tables

List of Figures

Abstract

INTELLIGENT SELECTION OF TRANSMISSION WAVEFORM FOR ACTIVE SONAR USING PREDICTED TARGET STATE

Venkata Sasikiran Veeramachaneni

George Mason University, 2019

Thesis Director: Dr. Jill K. Nelson

Underwater target tracking has vital importance in a variety of applications, most notably military surveillance and defense. This work is focused on underwater target tracking using active sonar. In active sonar, sound pulses are transmitted in water, and echoes produced by the target and any other obstacles are received by an array of hydrophones. The received echoes are processed to obtain estimates of object location and radial velocity, which form the input to a tracking filter for estimating the object's motion over time. The object location is given in terms of range and bearing (angle); the object's radial velocity, also known as range-rate, is obtained from the estimated Doppler shift.

In active sonar, the conventional sound pulses are the single-frequency continuous wave (CW) pulse and the frequency modulated (FM) pulse. These pulses differ from one another in terms of the range resolution they provide and whether or not they allow the system to measure Doppler shift. CW pulses allow for measurement of Doppler shift but have relatively poor range resolution. In contrast, a broadband FM pulse is insensitive to Doppler but has better range resolution than a CW pulse.

Reverberation is defined as the the reflection of sound energy toward the sonar system by objects other than the target of interest. Most active sonars operate in a reverberation-limited environment where an appropriate choice of sound pulse plays a key role in target tracking. If the target exhibits high Doppler at the time of sound pulse impingement, a CW pulse provides better tracking capability, while an FM pulse is more effective for a low Doppler target. A challenge, however, is that the target Doppler changes with time and is unknown at the time of waveform impingement. At present, the complementary strengths of CW and FM waveforms can be exploited only by an operator who actively chooses between them, which presents an unreasonable burden.

In this thesis, we devise and evaluate a decision algorithm that determines which waveform to transmit based on the target's predicted state. Building on the intuition of selecting a waveform based on the target's Doppler, we propose the Predicted State-Based Selection (PSBS) algorithm, which uses an estimate of the target's Doppler, derived from a state prediction produced by the tracking filter, to select the waveform for the next ping. A system consisting of a target path simulator, measurement data simulator, and tracking filter is modeled to conduct Monte Carlo simulations of PSBS. Its performance is evaluated by comparing it to the performance of transmitting either CW always or FM always. Simulation results show that the PSBS algorithm improves target localization estimates by 7.7% on average from the next best performing waveform selection approach, over all the turn-rates.

While PSBS improves significantly upon using only CW or only FM waveforms, it suffers substantial performance degradation for highly maneuvering targets. To address this shortcoming, this thesis suggests an enhancement to the PSBS approach; EPSBS (Enhanced PSBS) takes into account the number of measurements being considered by the tracker when making a waveform decision. Simulation results show that EPSBS eliminates the performance degradation observed for PSBS when targets undergo rapid maneuvers and improves the target localization estimates by 8.5% on average. Based on results obtained in this thesis, we conclude that intelligent selection of transmitted waveform can significantly improve tracking performance in active sonar.

Chapter 1: Introduction

A target, in general, is an object whose state is of interest to an observer. The state, in this sense, refers to the position, velocity, and other characteristics related to the motion of the target; it can change with time following dynamics that may be unknown. The target can follow various paths ranging from a straight line to complex maneuvers. Tracking the target has vital importance in a variety of applications, most notably military surveillance and defense. In target tracking, the state of a moving target is estimated, both at the current time and any point in the future, based on remote measurements. The measurements may be related to motion or attributes of the target, acquired by one or more sensors. This work is related to underwater target tracking.
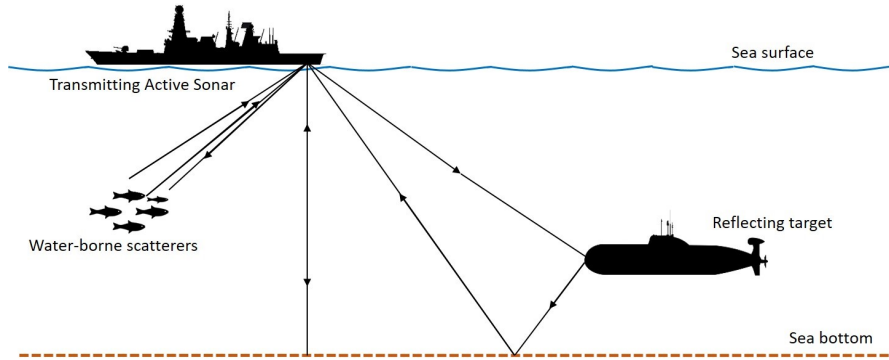
Figure 1.1: Scenario of active sonar transmitting a sound pulse into the ocean

In an underwater environment, sound waves are the only carriers that can propagate to remote distances, and hence they are widely used as a medium to acquire measurements for underwater target tracking. The systems that use sound waves to detect, locate and track a target are commonly called sonars (short for **So**und **N**avigation **A**nd **R**anging) [1]. There are two types of sonar: passive and active. Passive sonar tracks the target by listening to

the sound emitted by the target in the water. Active sonar tracks the target by emitting a sound pulse into the water and listening for the sound echo that bounces off of the target. This work is focused on underwater target tracking using active sonar.

Figure 1.1 shows the scenario of active sonar transmitting a sound pulse into the ocean. In active sonar, sound pulses are transmitted into the ocean where they collide with the target and any other obstacles along their propagation path and reflect back as echoes. The produced echoes are received by an array of hydrophones and are processed for object (obstacle) detection. The detections are associated with measurements containing an object's location and radial velocity; these measurements form the input to a tracking filter that estimates the object's motion over time [1, 2]. Figures 1.2a and 1.2b show the generic organization of an active sonar system and the inputs and outputs of a tracking filter, respectively.
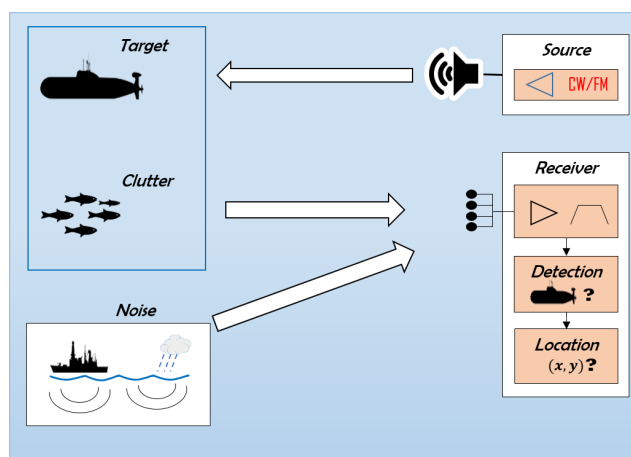
(a) Generic organization of an active sonar system [1]
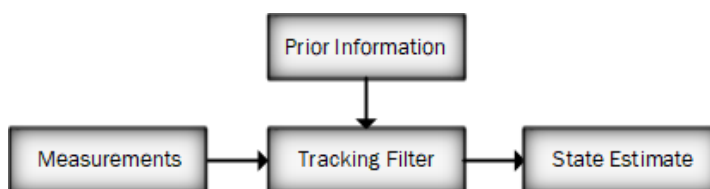
(b) Tracking filter block diagram

Figure 1.2: Target tracking with active sonar

The object location is given in terms of range and bearing where range (R) is the radial distance between the sonar platform and the object, and bearing (θ) is the direction of the object in radians or degrees in relation to the sonar platform [3]. The radial velocity, also known as range-rate $(\dot{r})$, is the rate at which the object moves away or toward the sonar platform; it is estimated from the observed Doppler shift [4]. More details on the range, bearing, range-rate, and Doppler shift can be found in section- 2.3.1.

1.1   Transmission Waveforms: CW and FM

(a) CW pulse in time domain   (b) CW pulse in frequency domain
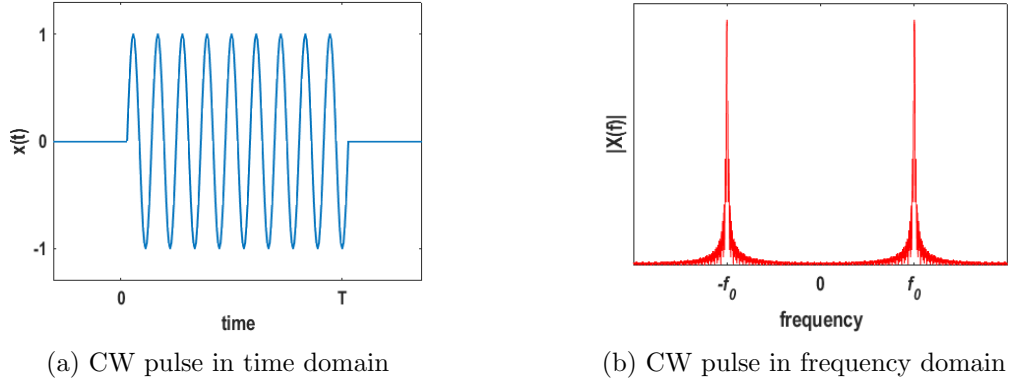
Figure 1.3: rectangular windowed CW pulse in time and frequency domain

In active sonar, the conventional sound pulses are the constant frequency continuous wave (CW) pulse and the frequency modulated (FM) pulse. The CW pulse, also known as a narrowband pulse, is a sinusoid of constant frequency f_0 enveloped by a window of time length T [1,5,6]. Figure 1.3 shows the simplest form of a CW pulse with a constant frequency f_0 limited by a rectangular envelope of duration T. An FM pulse, also known as a broadband pulse, is a sinusoid with frequency swept over a bandwidth B and enveloped by a window of time length T [1,5,6]. Figure 1.4 shows the simplest form of an FM pulse with frequency swept linearly over a bandwidth B and limited by a rectangular envelope of duration T.

(a) FM in time domain

(b) FM in frequency domain
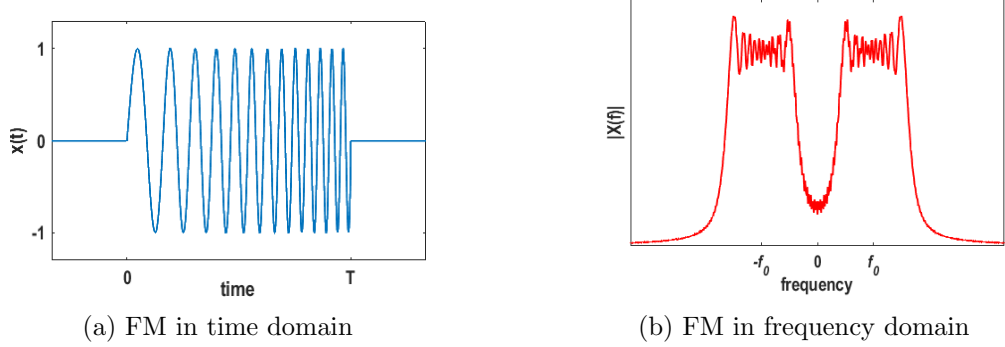
Figure 1.4: rectangular windowed FM pulse in time and frequency domain

CW and FM pulses differ from one another in terms of the range resolution they provide and their sensitivity to Doppler shift. Range resolution (ΔR) refers to the minimum separation required between closely spaced targets on the same bearing (i.e., at the same angle) for successful individual detection [3]. For a CW pulse, the range resolution is given as

$$\Delta R_{cw} = \frac{cT}{2}, \tag{1.1}$$

where c is the velocity of sound [3, 7]. For an FM pulse, the range resolution is given as [3, 7]

$$\Delta R_{fm} = \frac{c}{2B} \tag{1.2}$$

In an FM pulse, the pulse-length-modulation bandwidth product is usually much greater than unity ($BT >> 1$), and hence the range resolution for an FM pulse can be bounded as [6, 7]

$$\Delta R_{fm} << \frac{cT}{2} = \Delta R_{cw}. \tag{1.3}$$

From (1.3), for an equal pulse length, an FM pulse has much better range resolution compared to a CW pulse.

The narrow frequency band of a CW pulse is distorted by the Doppler shift. Hence a CW pulse is sensitive to Doppler, and its Doppler resolution is inversely proportional to the pulse length [7]. In contrast, an FM pulse has a much wider bandwidth, and its power spectrum is almost unchanged by the Doppler effect even though there is considerable frequency shift [1,6]. Hence, the FM pulse is insensitive to the Doppler shift, and its Doppler resolution is virtually non-existent. Therefore, with FM pulse transmission, an object's Doppler shift information cannot be extracted, and in turn, estimation of range-rate is not feasible

The above discussion has direct implications for the nature of the input to a tracking filter. When a CW pulse is transmitted, the tracking filter receives a three-dimensional input containing estimates of range, bearing, and range-rate. When an FM pulse is transmitted, the tracking filter receives a two-dimensional input containing estimates of only range and bearing.

1.2 Waveform Selection Considerations

Reverberation or clutter is defined as echoes caused by the reflection of the transmitted sound pulse by the surface and bottom boundaries, as well as obstacles in the path [1,5,8]. Most active sonars operate in a reverberation-limited environment where noise is mostly composed of reverberation [9]. In general, in a reverberation-limited environment, fine range resolution is required to reduce the interference of reverberation with the echo of a low-Doppler target [6]. For a higher Doppler target, Doppler shift in the received echo can be used to separate the target echo from reverberation if a Doppler sensitive pulse is used [6]. From the previous section, it is evident that neither a CW nor an FM pulse can resolve the range and Doppler shift simultaneously. Therefore, the choice of a transmission waveform, keeping the target's Doppler in mind, is crucial for target detection and tracking, which in turn impacts the overall system tracking performance.

However, the target's Doppler is not known at the time of waveform transmission and

moreover, the target's Doppler may change from time to time as underwater targets often have considerable maneuverability. At present, the complementary strengths of the waveforms can be exploited only by an operator who actively chooses among them, and the operator may not be able to make a choice for each ping as this presents an unreasonable burden. Hence, the choice of the best waveform for different detection and tracking scenarios has been a long-term problem for active sonar operators.

1.3 Proposed Approach: Predicted State Based Selection (PSBS)

The previous section highlights the challenge of choosing between CW and FM sonar pulses in a reverberation-limited environment. In this work, we address the problem of designing a waveform selection algorithm that predicts which pulse to send at the next transmission instant based on the target's predicted state. To be more precise, as the transmitted waveform determines the dimensionality of the input to the tracking filter, we devise an algorithm that determines whether to provide three-dimensional or two-dimensional input to the tracking filter based on the predicted state.

The tracking filter predicts the target's state at a future time instant. As the true Doppler of the target is not available, we propose a predicted state based selection (PSBS) approach wherein the waveform decision is made based on the radial velocity estimated from the target's predicted state. Given a predicted state $\hat{x}(k+1|k)$, the radial velocity (velocity component along the line of sight V_{los}) and the velocity component V_{orth} orthogonal to V_{los} are computed. If $V_{los} \geq V_{orth}$, a CW pulse is chosen for transmission; otherwise, an FM pulse is selected. Therefore, the PSBS approach establishes a feedback loop between the tracking filter and the active sonar system as shown in Figure 1.5
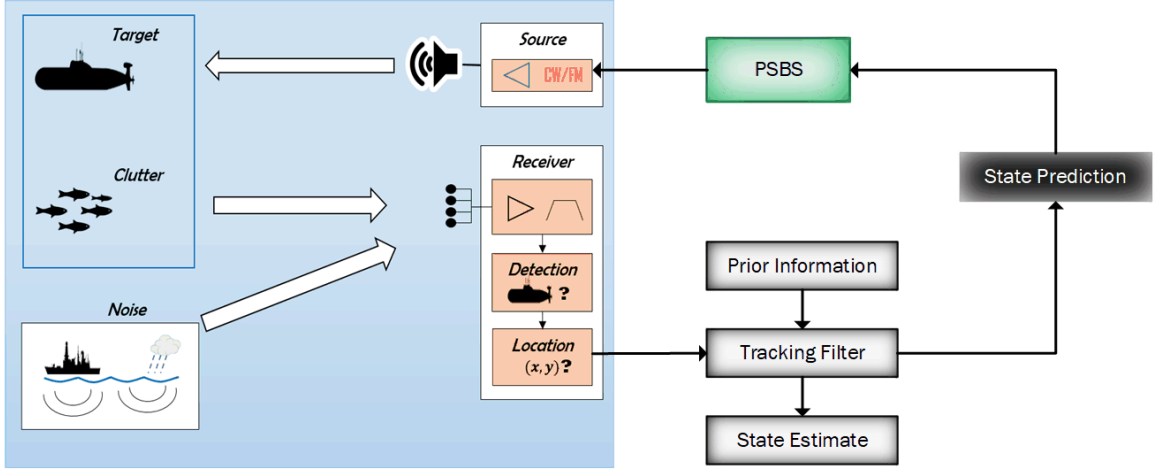
Figure 1.5: Establishment of feedback loop between the tracking filter and active sonar system

1.4 Objectives

The specific objectives of this thesis are:

- Model a system consisting of a target path simulator, measurement data simulator, and tracking filter- Probability Data Association Filter based on Unscented Kalman Filter (UKF-PDAF)

- Evaluate the performance of the proposed PSBS approach and alternative approaches (All-CW, All-FM) in terms of target in-track percentage and position root means square error using Monte Carlo simulations.

- Analyze the performance of PSBS performance, identify any shortcomings, and suggest enhancements to overcome those shortcomings.

1.5 Organization

The following thesis document is organized into six chapters. Chapter 2 provides the background required for a better understanding of the thesis topic. It mentions sound wave and its characteristics, and Doppler effect in them. It also overviews the signal processing

chain in active sonar and tracking filter. Chapter 3 reviews literature related to waveform optimization and cognitive detection systems. Chapter 4 defines and models the target path simulation, observation data simulation, and tracking filter. Chapter 5 describes the PSBS approach and analyzes its performance. It also highlights the PSBS approach shortcomings and discusses an enhanced version of PSBS approach. Chapter 6 contains a brief conclusion to the thesis and provides further directions for research.

Chapter 2: Signal Processing Chain in Active Sonar & Tracking Filter

This chapter provides background on using sound for ocean surveillance, describes the signal processing chain in active sonar, and discusses the tracking filter. The first section provides a short overview of sound propagation in water, Section 2.2 presents the active sonar signal processing chain and briefly describes each element, and the final section discusses the data association and state estimation tasks that comprise the tracking filter.

2.1   Sound Propagation in the Ocean

Electromagnetic waves act as a powerful tool in exploring and monitoring the environment to greater distances as they propagate unhindered in vacuum and air. However, due to strong conductivity and high dissipation in ocean water, electromagnetic waves are attenuated rapidly which limits their range and usefulness [1,5]. Sound waves are the only carriers that can propagate to remote distances in underwater; this is due to the low rate of absorption of sound energy and the presence of natural oceanic waveguides [10].
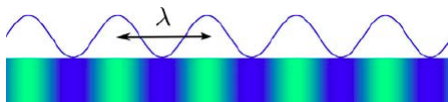
Figure 2.1: Sound wave propagation as a longitudinal wave [3]

A sound wave originates when a material or object vibrates, thereby creating vibrations in the surrounding medium [11]. In water, the vibrations propagate away from the

source as a longitudinal wave which is a combination of high and low-pressure areas called compressions and rarefactions. Figure 2.1 shows sound propagation as a longitudinal wave. The longitudinal waves are characterized by the wave period T, frequency f, sound speed c, and wavelength λ [3]. The speed of sound in seawater varies with depth but can be approximated as 1500 m/s. The wavelength (λ), speed (c), and frequency (f) are related as $\lambda = \frac{c}{f}$.

2.1.1 Doppler shift

When there is relative motion between the sound source and the sound receiver in the Line-Of-Sight (LOS) direction, there is a change in the frequency of the sound observed by the receiver. This phenomenon is called the Doppler effect. When a receiver is moving toward or away from a fixed sound source with a velocity component $v_{r_{los}}$ in the LOS direction, the observed frequency at the receiver (f_r) is given by

$$f_r = f_s \frac{c \pm v_{r_{los}}}{c},\tag{2.1}$$

where f_s is the frequency of the sound source [4]. In (2.1), $v_{r_{los}}$ is added if the receiver is moving toward the source (closing); $v_{r_{los}}$ is subtracted if the receiver is moving away from the source. The difference between the source frequency (f_s) and the received frequency (f_r) is known as the Doppler shift Δf. With Δv as the relative velocity component along the LOS, the Doppler shift is given by $\Delta f = f_s \frac{\Delta v}{c}$ [4].

A special case of interest is the Doppler shift for a target echo where the sound emitted from the source impinges on the target and echoes back to the receiver located on the same platform as the source. (This is known as a monostatic sonar system.) The Doppler shift in this case can be given as $\Delta f = 2f_s \frac{\Delta v}{c}$ [1,8].

2.2 Signal Processing in Active Sonar

In active sonar, a sound pulse is emitted by a set of transducers (underwater speakers). The emitted signal bounces off obstacles, and the reflections are sensed by an array of hydrophones (receivers). Each hydrophone converts the acoustic pressure into an electrical voltage, and the output voltages of the hydrophones are provided as input to a signal processing chain where the signals are filtered, enhanced, and combined in a suitable fashion for obstacle detection and localization [12]. Figure 2.2 shows the high-level block diagram of the active sonar signal processing chain.
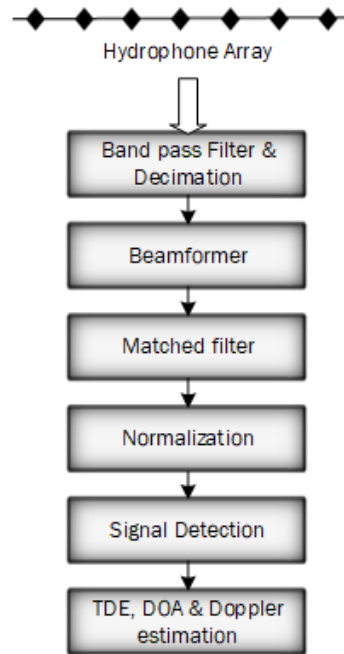
Figure 2.2: Signal processing chain in active sonar where TDE refers to time delay estimation and DOA refers to direction of arrival [3, 13].

A primary aim of the signal processing is to increase the signal-to-noise ratio by filtering out sound from unwanted frequencies and unwanted directions. Before any such enhancement begins, the analog voltage signals are passed through an anti-aliasing filter and then

sampled. The digitized signals are passed through a bandpass filter to remove out-of-band noise. The filtered signals are then shifted to baseband and decimated. The decimated signals are beamformed to determine the directions from which echoes have arrived. Beamforming is a spatial filtering technique where the signals from the hydrophones in the array are weighted, delayed, and summed to emphasize signals from certain directions while attenuating interference from other directions. The beamformer generates a set of beams in the search space, or in the favored directions which are passed to the matched filter to further increase the signal-to-noise ratio.

Matched filtering is the process of increasing the signal-to-noise ratio of the received signal by correlating it with a replica of the transmitted signal. For Doppler sensitive waveform, correlation loss occurs with the deviation of frequency in the received signals. Hence, Doppler-shifted replicas of the transmitted waveform are used for correlation. The matched-filtered output is normalized with an estimated mean reverberation and background noise power before proceeding to signal detection in order to reduce the background interference.

In the signal detector, the normalized matched filter output is compared against a detection threshold to decide whether or not a target echo is present. The detection threshold is chosen to satisfy specified detection and false alarm rates. Each detection is associated with a time delay estimation (TDE), direction of arrival (DOA), and Doppler shift. The time instant of the detection with a peak above the threshold corresponds to the time delay of the echo. The beam that resulted in detection gives the direction of echo arrival. The frequency shifted replica used in the matched filtering which resulted in the detection determines the Doppler shift in the received echo [13].

2.3   Tracking Filter

Target tracking is the process of estimating the state of a moving target at the current time, and/or predicting the state of the target at a future time, based on the acquired measurements. The measurements have uncertainty in their values due to presence of noise, as well as uncertainty in their origin since some echoes are generated by objects other

than the target of interest (clutter). The tracking filter includes both data association and state estimation. Data association resolves the measurement origin uncertainty, and state estimation estimates the target state by filtering the measurements provided. Figure 2.3 shows a block diagram of the tracking filter where the measurements (both target- and clutter-generated) are fed as input to the tracking filter.
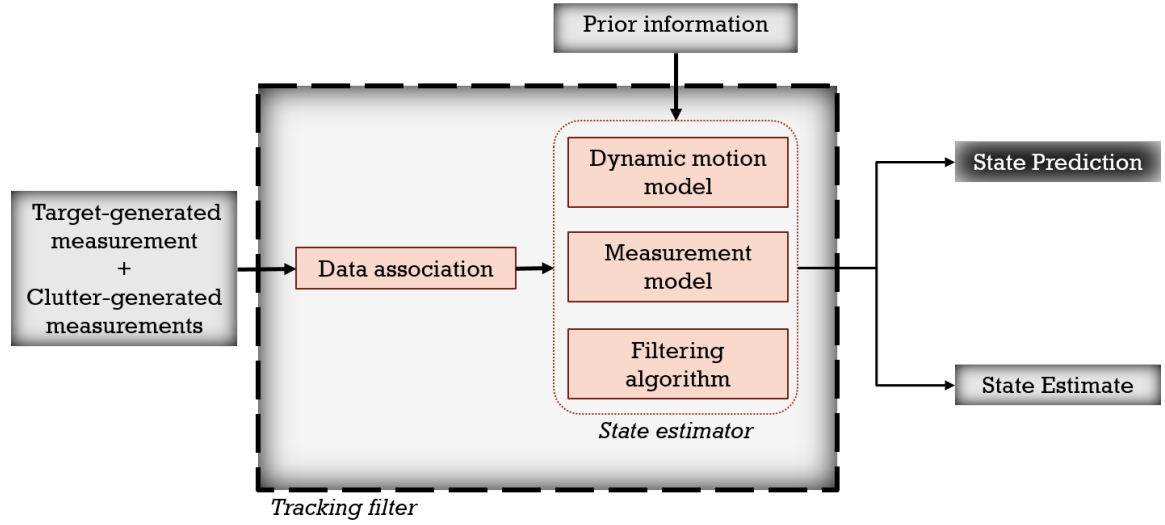
Figure 2.3: Tracking filter block diagram

In the tracking filter, the group of measurements is first subjected to data association, where single best measurement or its equivalent is extracted and provided as input to the state estimator. The state estimator, using prior information and with the help of a defined dynamic motion model and measurement model, predicts the target state and updates the prediction based on the current measurement. More details on the inputs to the tracking filter, state estimations, and data association are discussed in the following subsections.

2.3.1 Inputs to the tracking filter

Each measurement input to a tracking filter is multi-dimensional vector made up of range, bearing, and possibly range-rate (present only when CW is transmitted). The elements in the measurement vector are estimated based on the observations of time delay, direction of arrival, and Doppler shift.

The range is defined as the radial distance between the sonar platform and the object, and it can be estimated from the observed time delay between the transmitted pulse and the received echo. With τ as the observed time delay, the range of the object is given as $R = \frac{c\tau}{2}$ The observed time delay has variance inversely proportional to the square of the effective bandwidth of the transmitted signal. Therefore, the accuracy of the measured range is also dependent on the type of transmitted waveform.

Bearing is defined as the angle of the object in radians or degrees relative to the sonar platform. It is equal to the direction of arrival observed after beamforming in the signal processing chain. The accuracy of the bearing measurement is dependent on the effective length of the hydrophone array and the frequency of the transmitted waveform.

The radial velocity, also known as range-rate, is defined as the rate at which the object moves away from or toward the sonar platform. The measurement of range-rate is dependent upon the transmitted sound pulse Doppler sensitivity. With transmission of a Doppler-sensitive sound pulse, the Doppler shift information can be extracted and the range-rate, in the case of stationary sonar platform, is estimated as $\dot{r} = \frac{c\Delta f}{2f_s}$. The observed frequency shift has variance inversely proportional to the square of the effective pulse duration. Hence, the accuracy of the range-rate measurement depends on the transmitted pulse length.

2.3.2 Data association

In many tracking environments, it is common to have false contacts in the data acquired by the sensors, which leads to the input of multiple measurement vectors to the tracking filter. As discussed above, the state estimator works with only a single measurement, and hence data association techniques are required to produce a single measurement from the

group of observations at each time instant.

Data association is defined as selecting (or generating) a measurement from several candidates to feed to the state estimator. As a first step, a gate is established in the measurement space to isolate the most probable candidates from the group of measurements. This gate defines what is called the validation region, and it is constructed to guarantee that the target-generated measurement falls in the gate with a set probability known as the gate probability (P_g). When the gate probability is chosen close to be close to 1, the gate may contain more than one measurement, and association uncertainty arises.

Data association filters are required to extract or construct a single measurement from the multiple measurements in the validation gate. The simplest possible data association approach is the Nearest Neighbor Standard Filter (NNSF). NNSF selects the validated measurement that is closest to the predicted measurement and uses it in the state estimator to produce the target state update. A drawback of this approach is that it ignores the non-selected measurements; if the selected measurement is a spurious one, the tracking filter is likely to lose the target track. A more sophisticated and generally better performing approach for tracking a single target in clutter is the Probabilistic Data Association Filter (PDAF). PDAF assigns an association probability to each validated measurement and weights the measurements by these probabilities to form a single measurement as input to the state estimator. This work uses PDAF for data association, as discussed in further detail in Section 4.3.

2.3.3 State estimation

The state estimation algorithm processes a noise-corrupted measurement to estimate the target state in the presence of target model uncertainty. To any state estimator, the target dynamic motion model and measurement model (together called the state space model) are the main building blocks. The dynamic motion model is a mathematical model of the target's true motion behavior. With no prior knowledge of the target behavior, it is abstracted using generic motion models such as constant velocity, constant acceleration,

coordinated turn, etc., with white noise as input [14]. The closer the dynamic motion model to the behavior of the target, the better the state estimator estimates the target state.

The measurement model relates the target state to the observed measurement. Tracking systems often work with kinematic measurements, which are in the sensor measurement space, for state estimation. The sensor space may differ from the state space (e.g., polar vs. Cartesian space), and the measurement is related to the target state by the measurement model. The measurement model considered should also account for the measurement uncertainty resulting from noise corruption and inherent inaccuracy of the measurement devices.

Numerous state estimators with varying complexity are available in the literature. For a given tracking application, a suitable state estimator is chosen based on the nature of the state space model and the characteristics of the noise entering into the system. For single-target tracking problem with linear state space and additive Gaussian-distributed noise, the Kalman filter is the optimal linear minimum mean-squared error state estimator [15]. The Kalman filter is a recursive algorithm that can be subdivided into prediction and update phases. In the prediction phase, the target state for the next time instant is predicted using the dynamic motion model, and the predicted state is transformed into a predicted measurement by the measurement model. In the update phase, the predicted state is updated by the weighted difference between the predicted measurement and the observed measurement.

Many tracking applications possess non-linear state space models, and hence the classical Kalman filtering algorithm is no longer optimal. The extended Kalman filter (EKF) and unscented Kalman filter (UKF) are popular modifications to the Kalman filter designed to make the Kalman filter suitable for non-linear systems. The EKF is a suboptimal estimator which estimates the state using a first-order linearization of a non-linear function. The UKF, rather than linearizing the non-linear system, uses a deterministically selected set of weighted sample points, called sigma points, to propagate the statistical characteristics of random variables. Although the EKF is conceptually simple and widely used, it has

16

some significant drawbacks: Linearization may produce a highly unstable filter if the time-step intervals are not sufficiently small, and small time-steps require high computational overhead. Additionally, the EKF requires derivation of Jacobian matrices, which can be non-trivial and difficult to achieve in practical applications. In this work, the UKF is employed. The details of the UKF are provided in Section 4.3.

Chapter 3: Literature Review

In this chapter, we review the literature related to waveform selection and cognitive detection systems. Section 3.1 reviews the literature on waveform selection in relation to tracking performance improvement. Section 3.2 reviews the literature on cognitive radar and cognitive sonar.

3.1 Tracking Performance Focused Waveform Selection

In the conventional tracking system, where the sonar subsystem and the tracking filter are considered separate entities, the waveform selection was focused on obtaining maximum matched filter response. With the lack of flexibility in waveform generation, the early attempts of waveform design in connection to tracking performance improvement were focused at transmitted sound pulse amplitude modulation. In [16], the authors proposed an optimal radar signal amplitude modulation for a total energy and peak amplitude limited system, which is to alternate the transmitted signal between its peak-power and its zero-power levels.

With advancements in technology, detection systems such as active sonar and radar systems are capable of transmitting adaptively generated waveforms. In [17], the authors assumed a flexible waveform generator and reexamined the waveform selection problem as a waveform optimization problem with the overall tracking system performance as the cost function. The proposed tracking system has the tracking filter equations and performance measures (mean square tracking error and volume of the validation gate) explicitly dependent on the actual parameters of the transmitted waveform. The performance measures are minimized over the waveform parameters to form the best waveform for the next transmission, which establishes a feedback loop between the sonar subsystem and the tracking filter.

This approach is extended for tracking a single target in clutter by developing a waveform-selective probabilistic data association (WSPDA) algorithm in [18]. In this thesis, inspired by the idea of having tracking filter equations dependent on the waveform parameters, we developed the tracking filter algorithm with the measurement equation and measurement covariance dependent on the transmission waveform. However, the transmission waveforms are chosen based on the target and environment characteristics rather than in optimal fashion.

In the aforementioned works [17, 18], the tracking scenarios did not consider nonlinear measurement models and paid little attention to the FM waveforms. In [19], the authors propose an algorithm to select and configure linear and nonlinear FM waveforms to minimize the predicted mean square error (MSE) of the estimated target state in nonlinear measurement model scenarios.

The waveform optimization approaches discussed so far have dynamic adaption of transmission waveform. A non-dynamic and no feedback loop approach is presented in [20] which investigates and compares the performance of the fused CW and FM waveforms, with respect to tracking error, to homogeneous pulses (CW and FM) with the same energy. The authors propose that an equal division of energy between the positive sweep rate FM and the negative sweep rate FM, in a fused waveform, is the best choice. However, this work did not consider the effect of waveform fusion on sonar detection and estimation in the presence of clutter. In [21], the result of waveform fusion in the presence of range-rate dependent clutter was studied and proposed that the CW and FM fused waveform yields improvement over the unfused case for detection and tracking accuracy.

3.2   Cognitive Detection Systems

Traditional detection systems employ a feed-forward processing chain in which the receiver data is processed to extract the target information for achieving a system objective. The

work of Kershaw and Evans in [17] prompted the evolution of detection systems into adaptive models where a feedback loop between the receiver and the transmitter was added. The added feedback loop facilitated the systems in making intelligent decisions about transmitted waveforms; however, the intelligence is limited by the lack of memory and learning from past experience, leaving room for improvement to a full-fledged intelligent system. A truly intelligent system observes the environment and mimics human cognition in planning the next action by predicting the consequences of actions, learning from the environment, and storing the learned knowledge. Next-generation detection systems providing enhanced information-processing power, robust operation via intelligent actions, and a higher degree of autonomy can be achieved by embedding cognitive abilities, and such systems are called cognitive detection systems. In this section, the literature related to cognitive detection systems, specifically cognitive radar and cognitive sonar, is reviewed.

3.2.1 Cognitive radar

Radar, short for **R**adio **D**etection **A**nd **R**anging, is a remote-sensing system that sends out high frequency electromagnetic waves to detect and track targets. Inspired by the echolocation system of the bat, Haykin introduced the concept of cognitive radar constituting three basic ingredients: intelligent signal processing, feedback from the receiver to the transmitter, and radar returns information preservation [22]. Haykin also categorized cognitive radar systems depending on whether the information leading to cognition resides inside or outside the receiver. Outside-in cognitive radar systems have short-term memory which is developed on the fly whereas inside-out cognitive systems have prior knowledge of the environment which is embedded into the receiver. The knowledge-based radar system discussed in [23] is an inside-out cognitive radar system where the signal processing chain is adapted based on the information retrieved through prior experimentation using a knowledge base. Another inside-out cognitive radar system architecture integrating knowledge-aided processing and adaptive transmit radar technologies is discussed in [24].

Fueled by the analogy between the human brain and radar, Haykin describes a cognitive radar that emulates the visual brain for realizing cognition in [25]. In this paper, the cognitive radar design is focused on embodiment and implementation of the four relevant building blocks (perception-action cycle, memory, attention, and intelligence) of the cognition model proposed by Fuster [26]. Haykin also establishes a clear distinction between traditional radar, fully adaptive radar, and truly cognitive radar where the cognitive radar exploits local and global feedback loops between the receiver and transmitter. He also presents experimental results showcasing the progressive improvement of a radar system's tracking capability with increasing degree of cognition. In [27], the work in [17], [19], [22], [25] is generalized and formalized to develop a general cognitive radar framework for a radar system that can perform target detection and tracking. The work in [28] argues that the cognitive characteristic of anticipation can also enhance the radar system tracking performance by using a partially observable Markov decision process (POMDP) in radar management.

3.2.2 Cognitive sonar

Even though the introduction of cognitive radar by Haykin motivated research in the field of cognitive sonar, it has not drawn as much attention in the research community. Initial work related to cognitive sonar is presented in [29], where the cognitive sonar approaches are proposed for harbor and maritime surveillance applications. The proposed cognitive MIMO sonar facilitates a cognition module consisting of prior knowledge and online learning of the environment for robust target detection. In [30], Xiaohua investigated the application of cognition in sonar by performing adaptive beamforming with prior knowledge of interfering sources. Later, in [31], he proposed a more detailed cognitive sonar concept which embodies a receiver-transmitter feedback loop, prior knowledge, and environmental perception. A proof-of-concept cognitive sonar is presented in [32]. The proposed cognitive sonar dwells in scan mode, where an FM is always sent, and switches to adaptive mode to enhance target detection, where a CW is sent and/or transmit beamforming is performed when the target's

track-quality score obtained from the tracking layer is low.

In contrast to the adaptive systems discussed so far, a cognitive sonar model based on the goal-driven autonomy (GDA) framework, borrowed from the artificial intelligence area, is proposed in [33] which can tune both the receiver and transmitter for better surveillance and tracking. The proposed cognitive sonar model is demonstrated by studying a waveform selection problem where the transmit waveform is selected based on a maneuvering target's estimated radial velocity. Motivated by this approach, in this thesis, we address the waveform selection problem, for better tracking performance, by proposing algorithms that select transmit waveforms based on the maneuvering target's predicted radial velocity and the number of clutter points present in the validation gate.

Chapter 4: Tracking System Modeling

In Section 1.3, we proposed a waveform selection approach in which a feedback loop is established between the tracking filter and transmitter of the sonar system. To evaluate the performance of the proposed algorithm, Monte Carlo simulations are performed, and hence a mathematical model of the sonar system and tracking filter must be developed. From Figure 1.2a, we see that the sonar system takes as input which pulse to transmit and produces estimated measurement data; from Section 2.3, it is evident that the tracking filter takes in measurement data as its only input. Therefore, the simplest way to abstract the sonar system behavior is by a measurement data simulation block which can generate data relevant to different types of transmission waveforms. This chapter discusses in detail the simulation of measurement data and a tracking filter algorithm.

Measurement data consists of target-generated and clutter-generated measurements, the former requiring modeling of a target path. In Section 4.1, target behavior is defined and modeled using constant velocity and coordinated turn motion models. In Section 4.2, the modeling of target- and clutter-generated measurements is discussed in detail. Section 4.3, presents the tracking filter algorithm and its elements such as the state space model, state estimator, and data association filter.

4.1   Target Path Simulation

Underwater targets may exhibit straight-line or maneuvering motion. The maneuvering motion involves changing the course of travel by ascending, descending, or turning and changing speed. The focus of this research is predicting waveforms to be transmitted at the next ping based on the estimated Doppler of the target. Thus, to assess the performance of the waveform preidiction approach, the desired target behavior should exhibit varying

Doppler content which can be obtained by performing maneuvers. For this research, we assume that target motion is limited to a horizontal plane and that the target travels at a constant speed, though the direction of travel may change to produce the turning maneuvers. These assumptions not only achieve desired target behavior but also keep the target path generation simple and requires a less complex tracking filter for better target tracking.

In our model, the target travels from a location at a certain distance from the sonar platform directly toward the platform. At randomly-generated times (described further below), the target makes a maneuver (can be positive or negative based on the change in direction heading) with a deterministic turn rate, significantly altering the direction of travel and the Doppler content. Figure 4.1 shows two sample realizations of the target path generated.

In Figure 4.1a, a target path is simulated for 400 seconds. The path starts at position $(7211m, 33.69°)$ and heads straight toward the sonar platform with a speed of 30 m/s. The path has five maneuvers: the first, third, and fifth are positive maneuvers, and the second and fourth are negative maneuvers. A positive maneuver changes the target's direction of motion in a counter-clockwise direction by a randomly-generated deviation angle. The deviation angle in a positive maneuver is modeled as a realization of a Gaussian random variable with a mean of 90° and a standard deviation of 10°. A negative maneuver modifies the target's direction of travel as needed to align the target's motion direction along the line-of-sight (LOS) to the sonar platform.

In both maneuvers, the required deviation angle is achieved at a constant turn rate of 3°/sec. The positive and negative maneuvers alternate and are spaced in time by randomly-generated intervals. The time intervals are modeled as realizations of inverse Gaussian random variables with mean $(\mu) = 60$ and shape parameter $(\lambda) = 60$. The probability density function of inverse Gaussian random variable is shown in Figure 4.2.

From the previous discussion, it is clear that each generated path consists of straight line trajectories and maneuvering segments, each of which can be generated from their corresponding motion models. In two-dimensional space, the target state at time k is
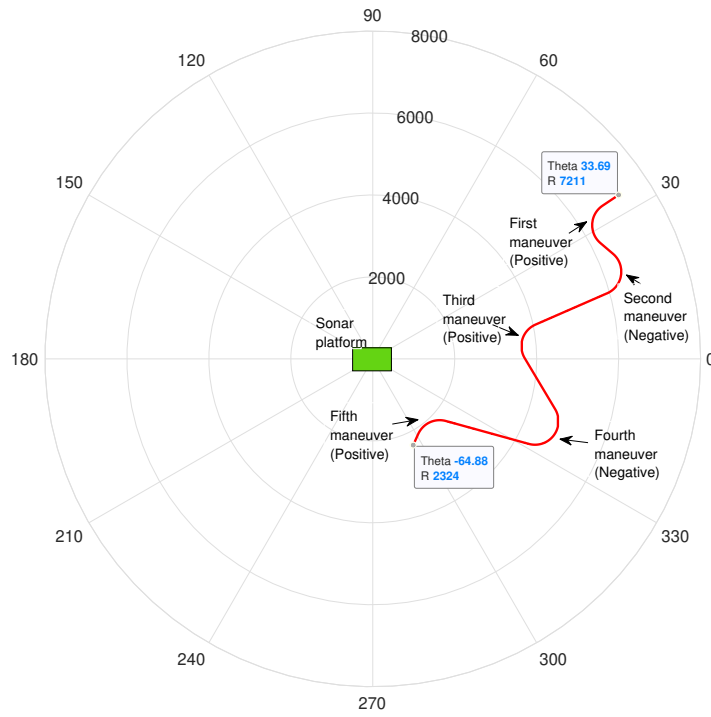
(a) Target path with turn rate of 3°/sec
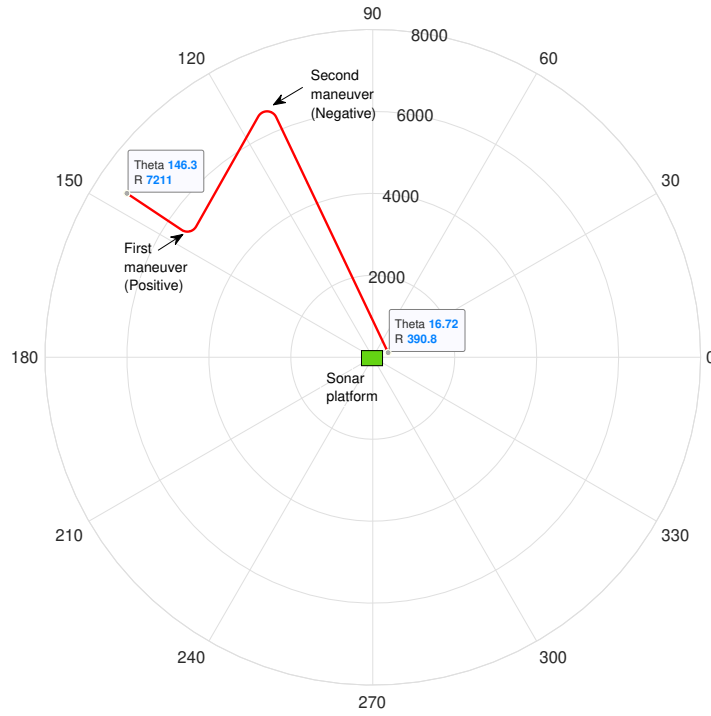
(b) Target path with turn rate of 7°/sec

Figure 4.1: Two realizations of the target path.
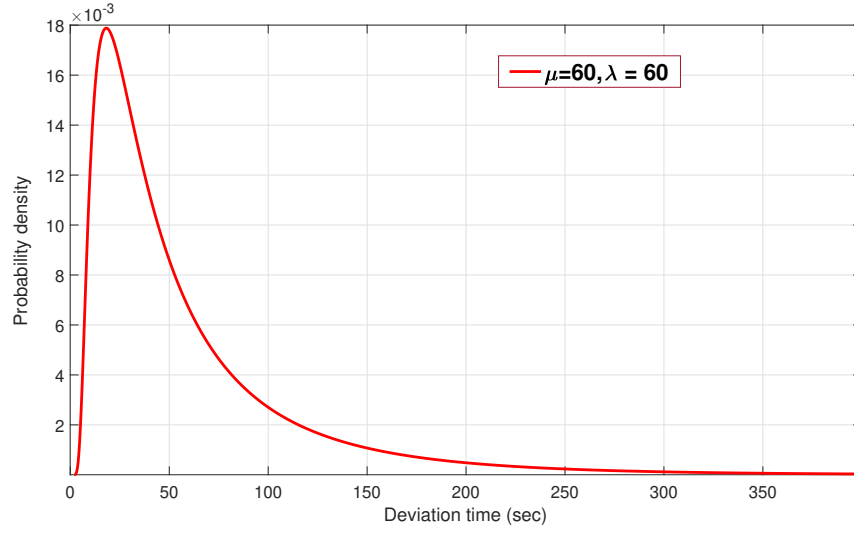
Figure 4.2: Inverse Gaussian probability density function for mean $(\mu) = 60$ and shape parameter $(\lambda) = 60$

denoted as $x(k) = [x_k \ y_k \ \dot{x}_k \ \dot{y}_k]'$, where x_k, y_k represents target position in Cartesian coordinates at time k and $\dot{x}_k, \dot{y}_k$ corresponds to target velocity at time k. f is the frequency at which target state values are generated and is chosen as 1000Hz. The target's straight-line trajectory is generated using the constant velocity motion model given below.

$$\begin{bmatrix} x_{k+1} \\ y_{k+1} \\ \dot{x}_{k+1} \\ \dot{y}_{k+1} \end{bmatrix} = \begin{bmatrix} 1 & 0 & \frac{1}{f} & 0 \\ 0 & 1 & 0 & \frac{1}{f} \\ 0 & 0 & 1 & 0 \\ 0 & 0 & 0 & 1 \end{bmatrix} \begin{bmatrix} x_k \\ y_k \\ \dot{x}_k \\ \dot{y}_k \end{bmatrix} \tag{4.1}$$

The maneuver trajectories can be described as target motion at a constant speed in circular segments around an imaginary center point. Hence, the maneuvers can be modeled using the coordinated turn dynamics given below, where ω denotes the turn rate of the

target and replacing it by $-\omega$ produces a negative maneuver.

$$\begin{bmatrix} x_{k+1} \\ y_{k+1} \\ \dot{x}_{k+1} \\ \dot{y}_{k+1} \end{bmatrix} = \begin{bmatrix} 1 & 0 & \frac{sin(\frac{\omega}{f})}{\omega} & \frac{cos(\frac{\omega}{f})-1}{\omega} \\ 0 & 1 & \frac{1-cos(\frac{\omega}{f})}{\omega} & \frac{sin(\frac{\omega}{f})}{\omega} \\ 0 & 0 & cos(\frac{\omega}{f}) & -sin(\frac{\omega}{f}) \\ 0 & 0 & sin(\frac{\omega}{f}) & cos(\frac{\omega}{f}) \end{bmatrix} \begin{bmatrix} x_k \\ y_k \\ \dot{x}_k \\ \dot{y}_k \end{bmatrix} \tag{4.2}$$

Target path generation algorithm flowchart

Figure 4.3 presents a flowchart for the target path generation model. The main segment of the algorithm is the loop which generates the path iteratively using the target motion models discussed in (4.1) and (4.2). At any given instant, the path generation model will be in either constant velocity state or maneuver state. Initially, the path generation model is in the constant velocity state. In constant velocity state, the model iteratively generates the next target state from the last generated state using (4.1) until the generated state is out of the surveillance region, the time interval indicates that a maneuver should begin, or the simulation time has ended.

When it is time to make a maneuver, the model switches to maneuvering state. In this state, the model performs a positive maneuver if it is the first maneuver in the path or if the previous maneuver was negative; otherwise, the model performs a negative maneuver. The target deviation by a required angle is achieved at a specified constant turn rate. The model iterativley generates the next target state from the last generated state using (4.2) until the required deviation is achieved, the target state is outside the surveillance region, or the simulation time has ended. Once the model achieves the required deviation of the target, the model switches to the constant velocity state.
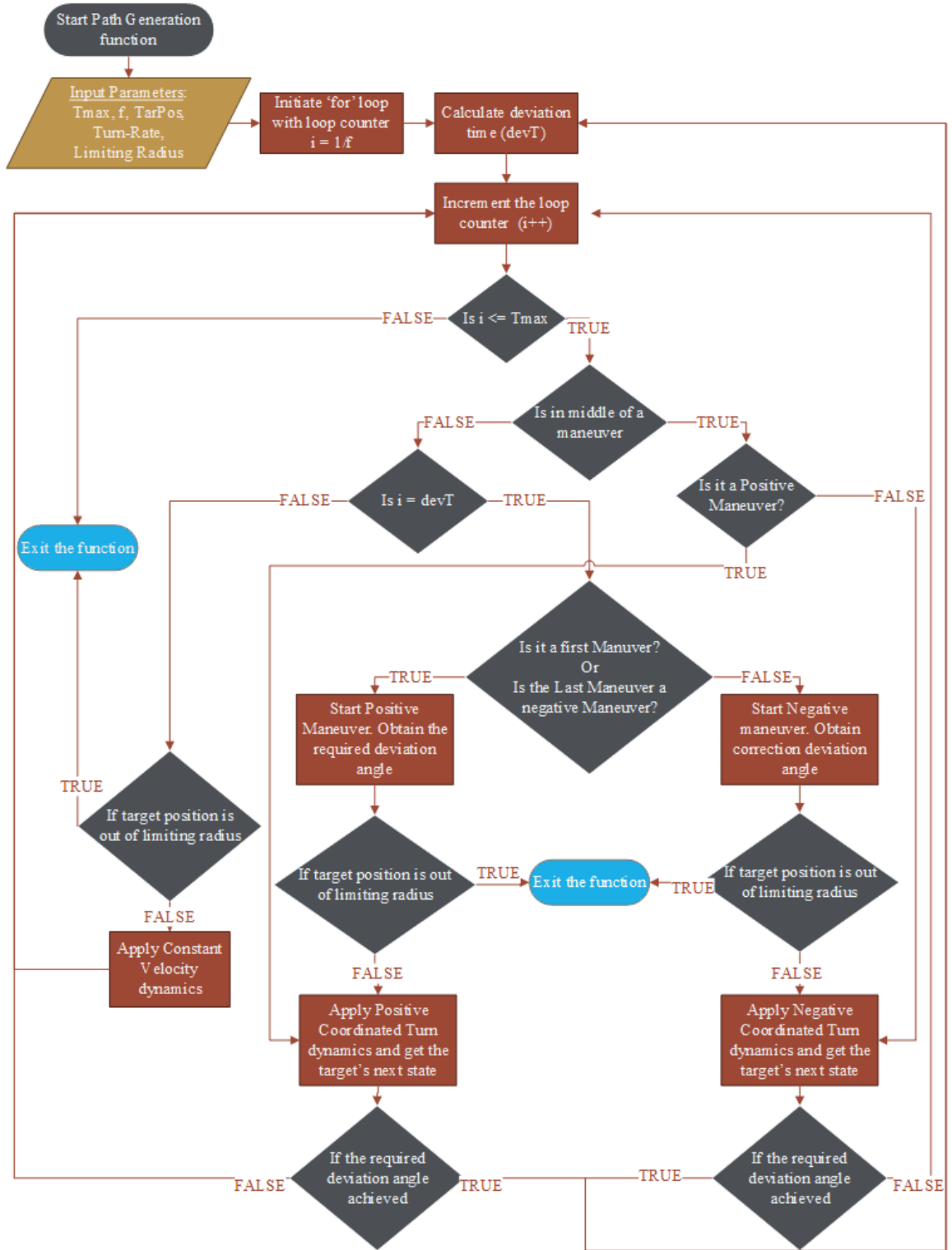
Figure 4.3: Flow chart of the target path generation process where $Tmax$ is the maximum path simulation time, f is the sampling frequency, $TarPos$ is the target position at the start of simulation

4.2   Measurement Data Model

The measurement data model, an abstraction of the sonar system behavior, simulates data which consists of target- and clutter-generated measurements appropriate to the transmitted waveform. These two types of measurements (target and clutter) are generated independently and are grouped into a single set of data before being passed to the tracking filter. Figure 4.4 provides a block diagram of the measurement data model with waveform decision input and measurement data output.
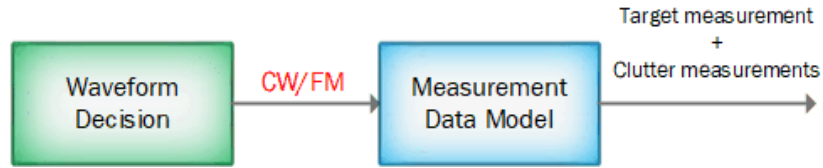
Figure 4.4: Block diagram of measurement data model

Target-generated measurements, discussed in detail in Section 4.2.1, are obtained by sampling the simulated target path and corrupting the transformed samples with Gaussian distributed noise. Two sets of target measurements are generated, one for each type of waveform, as the transmission waveform dictates the dimensionality and the accuracy of the measurements. Clutter-generated measurements, discussed in detail in Section 4.2.2, are realizations of a random variable uniformly distributed in the observation space.

The assumptions used in the simulation of measurement data are as follows:

- A single target is present in the surveillance area at any given time.

- The transmitted waveforms are long enough to completely insonify the obstacles, which are treated as point targets.

- Waveforms are transmitted every 2 seconds, and the echoes are received by the time of next transmission.

- Target echoes in consecutive transmission intervals contain the position of the target spaced apart by transmission time period.

4.2.1 Target-generated measurements

To obtain the target-generated measurements for a simulated path, the first step is to determine the target state at points 2 seconds apart on the target path. The target state is transformed into range, bearing, and range-rate. With the target state at time k as $x(k) = [x_k \ y_k \ \dot{x}_k \ \dot{y}_k]$, the range (r_k) can be calculated as

$$r_k = h_r(x(k)) = \sqrt{x_k^2 + y_k^2} \tag{4.3}$$

the bearing θ_k can be calculated as

$$\theta_k = h_\theta(x(k)) = \begin{cases} tan^{-1}\left(\frac{x_k)}{y_k}\right) & \text{if } y_k > x_k, \ x_k > 0 \\ \frac{\pi}{2} - tan^{-1}\left(\frac{y_k)}{x_k}\right) & \text{if } y_k < x_k, \ x_k > 0 \\ \pi - tan^{-1}\left(\frac{x_k}{y_k}\right) & \text{if } y_k > x_k, \ x_k < 0 \\ \frac{3\pi}{2} - tan^{-1}\left(\frac{y_k}{x_k}\right) & \text{if } y_k < x_k, \ x_k < 0 \end{cases} \tag{4.4}$$

and the range-rate $(\dot{r}_k)$ can be calculated as

$$\dot{r}_k = h_{\dot{r}}(x(k)) = \frac{x_k \dot{x}_k + y_k \dot{y}_k}{\sqrt{x_k^2 + y_k^2}} \tag{4.5}$$

The range, bearing, and range-rate are used to generate two versions of the target measurement, one for each transmission waveform. The CW version of the target measurement
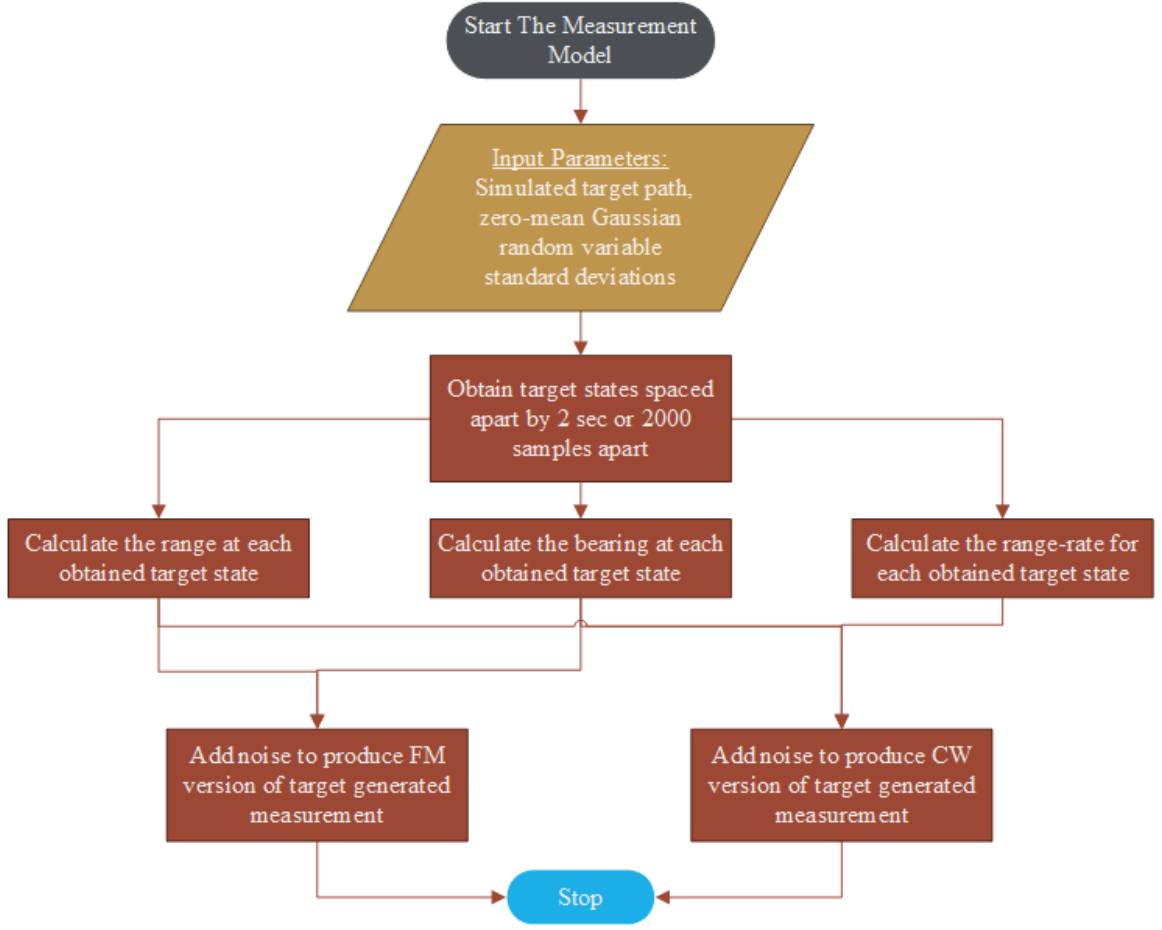
Figure 4.5: Flow chart of target-generated observation model

is a three-dimensional vector containing range, bearing, and range-rate corrupted by additive zero-mean Gaussian noise with standard deviations $\sigma_{r_{cw}}$, $\sigma_{\theta_{cw}}$ and $\sigma_{\dot{r}_{cw}}$, respectively. Similarly, the FM version of the target measurement is a two-dimensional vector containing range and bearing corrupted by additive zero-mean Gaussian noise with standard deviations $\sigma_{r_{fm}}$ and $\sigma_{\theta_{fm}}$, respectively. Table 4.1 shows one set of standard deviations for each element of the CW version and FM version target measurements used in the simulation results presented in this Thesis. Figure 4.5 shows the algorithm flowchart for simulating target-generated measurements.

Table 4.1: One set of noise standard deviation values for target-generated measurements

	CW	FM
σ_{Range}	$40m$	$10m$
σ_{Bearing}	0.01745rad (1°)	0.01745rad (1°)
$\sigma_{\text{RangeRate}}$	$0.5m/sec$	NA

4.2.2 Clutter-generated measurements
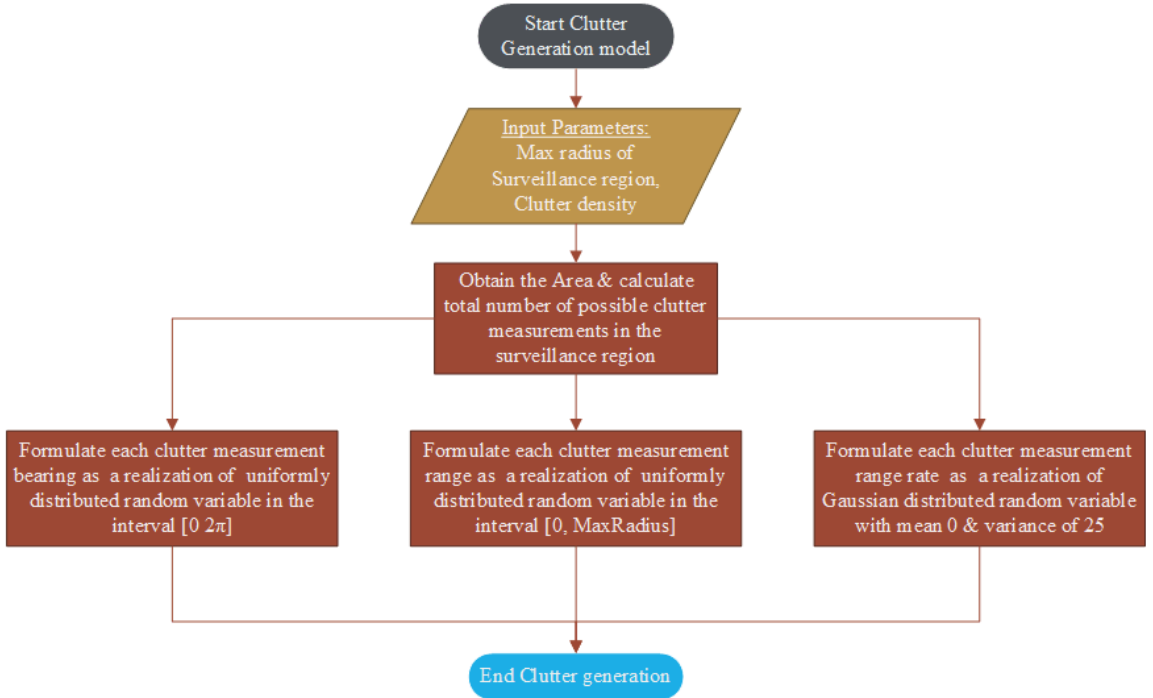
Figure 4.6: Flow chart for clutter generation model

In an active sonar system, echoes from obstacles other than the target are called rever-beration or clutter. If the reverberation is caused by the boundaries of the ocean, it is called surface and bottom reverberation and if it is due to fish, plankton, suspended particles or bubble clouds, it is called volume reverberation. In this research, we assume that only

volume reverberation is present and that the measurements resulting from it are uniformly distributed in polar space with a density of 10^{-5} measurements per unit search area.

In every transmission interval, the total number of clutter measurements that occur in the region is computed based on the maximum range ($MaxR$) of the surveillance region and on the clutter density. For each clutter measurement, the range and bearing are obtained as realizations of uniform random variables that take values in the intervals $[0 \; MaxR]$ and $[0 \; 2\pi]$, respectively. The range-rate for each clutter measurement is obtained as a realization of a zero-mean Gaussian random variable with a variance of 25. Figure 4.6 & Figure 4.7 present the flowchart of the clutter generation model and two sample realizations of the spatial distribution of clutter points in different transmission intervals, respectively. In case of an FM transmission, range-rate values in the clutter measurements are omitted.

4.3   Tracking Filter

The tracking filter is introduced in Section 2.3 with Figure 2.3 presenting a high-level block diagram. In this section, tracking filter components such as data association and state estimation are discussed in detail and specific to the tracking problem considered in this research. The dynamic motion model and measurement model, fundamental elements of state estimation, are discussed in Section 4.3.1 and Section 4.3.2, respectively. Section 4.3.3 presents the unscented Kalman filter (UKF), the state estimation algorithm chosen for this work. Finally, Section 4.3.4 details the probability data association filter for associating measurements with the target.

4.3.1   State space model: Dynamic motion model

The dynamic motion model is an abstraction of the target's motion behavior. The generic linear dynamic motion model can be given as

$$x(k+1) = Fx(k) + Bu(k), \tag{4.6}$$

(a)

(b)
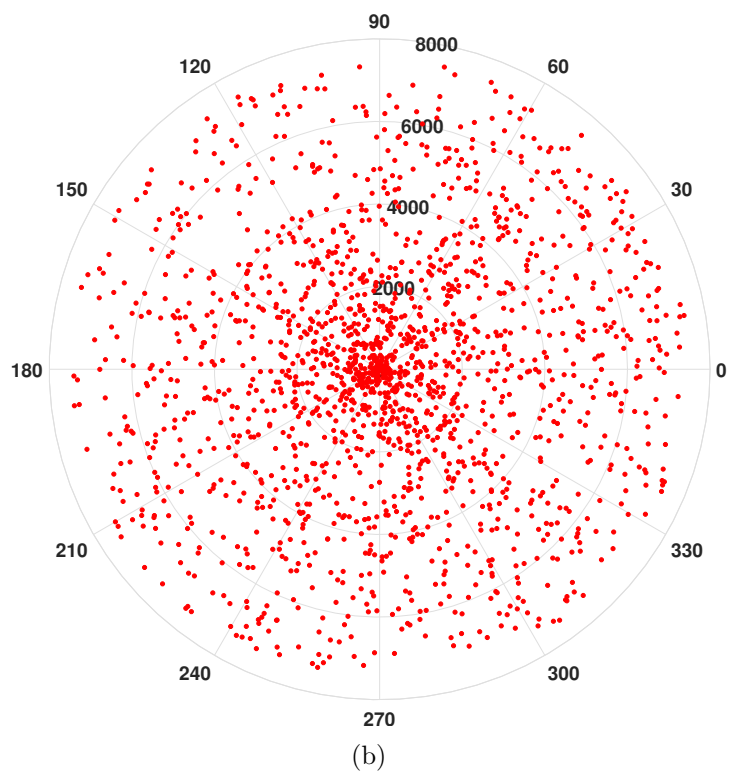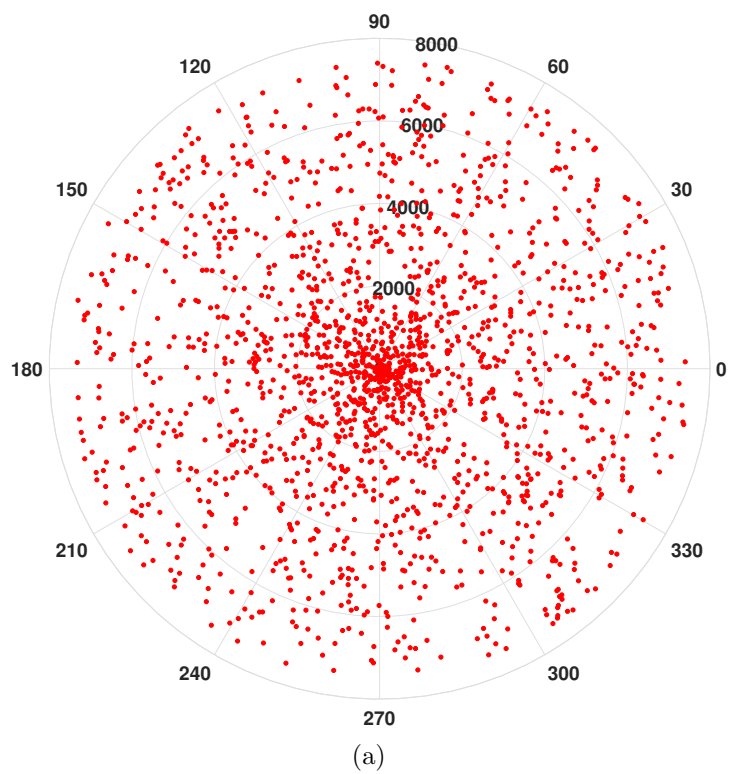
Figure 4.7: Two sample realizations of clutter or volume reverberation.

where $x(k)$ and $u(k)$ are the state vector and input vector, respectively, at time k. F and B are the state transition matrix and input-gain matrix, respectively. The simulated target behavior in Section 4.1 exhibits two kinds of motion: Constant velocity motion and coordinated turn motion. The two motions cannot be defined by a single state transition matrix (F). However, the maneuvers can be approximated as an input of white noise acceleration to a constant velocity system, and hence we can use a single linear dynamic motion model to approximate the simulated target behavior.

With the state vector $x(k) = [x_k \; y_k \; \dot{x}_k \; \dot{y}_k]'$ and zero-mean white noise vector $v(k) = [v_x \; v_y]'$ as input to the dynamic motion model, the state at time $k+1$ can be given as

$$x(k+1) = Fx(k) + \Gamma v(k), \tag{4.7}$$

where Γ is the input-gain or noise gain matrix, and

$$E[v(k)v(j)] = \begin{bmatrix} \sigma_{v_x}^2 \delta_{kj} & 0 \\ 0 & \sigma_{v_y}^2 \delta_{kj} \end{bmatrix}. \tag{4.8}$$

With T as the sampling or observation interval, the state transition matrix F is

$$F = \begin{bmatrix} 1 & 0 & T & 0 \\ 0 & 1 & 0 & T \\ 0 & 0 & 1 & 0 \\ 0 & 0 & 0 & 1 \end{bmatrix}, \tag{4.9}$$

and the noise gain matrix Γ is

$$\Gamma = \begin{bmatrix} \frac{T^2}{2} & 0 \\ 0 & \frac{T^2}{2} \\ T & 0 \\ 0 & T \end{bmatrix}. \tag{4.10}$$

The dynamic motion model in (4.7) is also called the discrete white noise acceleration model (DWNA). The model assumes that the target undergoes constant acceleration during the sampling period and the accelerations in different sampling periods is uncorrelated. The covariance of the process noise or input noise is given as

$$Q = E[\Gamma v(k) v(k)' \Gamma'] = \Gamma \begin{bmatrix} \sigma_{v_x}^2 & 0 \\ 0 & \sigma_{v_y}^2 \end{bmatrix} \Gamma'. \tag{4.11}$$

Judicious selection of σ_{v_x} and σ_{v_y} aids in better maneuver modeling; a practical range is $0.5a_{max} \leq \sigma_{v_x}, \sigma_{v_y} \leq a_{max}$, where a_{max} is the maximum acceleration possible along both axes during a maneuver at a particular turn rate [15] [34]. In this research, σ_{v_x} and σ_{v_y} are equally chosen equal to a_{max}. The look-up Table 4.2 presents a_{max} for the range of turn rates considered.

Table 4.2: Look-up table for maximum acceleration (a_{max}) along both axes during maneuvers as a function of turn rate

Turn-Rate (deg/sec)	1	1.5	2	2.5	3	3.5	4	4.5
$a_M(m/sec^2)$	0.52	0.79	1.05	1.31	1.57	1.83	2.09	2.36

Turn-Rate (deg/sec)	5	5.5	6	6.5	7	7.5	8	8.5
$a_M(m/sec^2)$	2.62	2.88	3.14	3.40	3.66	3.92	4.19	4.45

4.3.2 State space model: Measurement model

The measurement model establishes a relationship between the target state and the measurement; it also accounts for inaccuracy in the measurements due to noise. From the range, bearing, and range-rate transformation functions in (4.3), (4.4), & (4.5), respectively, it is clear that the target state and the measurement are non-linearly related. The generic nonlinear measurement model equation with measurement z_k at time k can be given as

$$z_k = h[x(k)] + w(k), \tag{4.12}$$

where h is the vector of non-linear functions (also called the measurement function) that transforms the state space vector into the measurement space, and w is an additive zero-mean Gaussian measurement noise vector with covariance $E[W(k)W'(j)] = R(k)\delta_{kj}$.

As discussed previously, the dimensionality and the accuracy of the measurements vary with the transmitted waveform. Therefore, two versions of the measurement model equations, one for each type of waveform, are considered in the development of the tracking filter. The CW version of the measurement model is

$$z_{k_{cw}} = h_{cw}[x(k)] + w_{cw}(k), \tag{4.13}$$

where

$$z_{k_{cw}} = \begin{bmatrix} r_{k_{cw}} \\ \theta_{k_{cw}} \\ \dot{r}_{k_{cw}} \end{bmatrix} ; \quad h_{cw}[x(k)] = \begin{bmatrix} h_r(x(k))) \\ h_\theta(x(k)) \\ h_{\dot{r}}(x(k)) \end{bmatrix} ; \quad w_{cw}(k) = \begin{bmatrix} w_{r_{cw}} \\ w_{\theta_{cw}} \\ w_{\dot{r}_{cw}} \end{bmatrix}, \tag{4.14}$$

and the measurement noise covariance matrix (R) for the above model is given as

$$R_{cw}(k) = \begin{bmatrix} \sigma_{r_{cw}}^2 & 0 & 0 \\ 0 & \sigma_{\theta_{cw}}^2 & 0 \\ 0 & 0 & \sigma_{\dot{r}_{cw}}^2 \end{bmatrix}, \tag{4.15}$$

where $\sigma_{r_{cw}}$, $\sigma_{\theta_{cw}}$, & $\sigma_{\dot{r}_{cw}}$ are the standard noise deviations in range, bearing, and range rate, respectively, when a CW waveform is transmitted.

The FM version of the measurement model is

$$z_{k_{fm}} = h_{fm}[x(k)] + w_{fm}(k), \tag{4.16}$$

where

$$z_{k_{fm}} = \begin{bmatrix} r_{k_{fm}} \\ \theta_{k_{fm}} \end{bmatrix} ; \quad h_{cw}[x(k)] = \begin{bmatrix} h_r(x(k))) \\ h_\theta(x(k)) \end{bmatrix} ; \quad w_{fm}(k) = \begin{bmatrix} w_{r_{fm}} \\ w_{\theta_{fm}} \end{bmatrix}, \tag{4.17}$$

and the measurement noise variance matrix (R) for the above model is given as

$$R_{fm}(k) = \begin{bmatrix} \sigma_{r_{fm}}^2 & 0 \\ 0 & \sigma_{\theta_{fm}}^2 \end{bmatrix}, \tag{4.18}$$

where $\sigma_{r_{fm}}$ & $\sigma_{\theta_{fm}}$ are the standard noise deviations in range and bearing, respectively, when an FM waveform is transmitted. While implementing the tracking filter, the noise standard deviation values in the CW and FM measurement models are chosen to be same as the standard deviation values used in generating the CW and FM target measurements in Section 4.2.1.

38

4.3.3 State estimator: Unscented Kalman filter (UKF)

The state estimator is chosen based on the nature of the state space model as well as the characteristics of the process noise and measurement noise entering into the system. From the dynamic motion model in (4.7) and the measurement model in (4.12), it is evident that the state space model is non-linear and the noise entering into the system is assumed to be Gaussian. Based on the discussion in Section 2.3.3, a suitable state estimator in this case is the unscented Kalman filter (UKF).

The UKF algorithm can be subdivided into a prediction segment and an update segment. In the prediction segment, the predicted mean $\hat{x}(k+1|k)$ and covariance $P(k+1|k)$ of the state $x(k+1)$ are obtained by transforming the sigma points (described in 2.3.3) with mean $\hat{x}(k|k)$ through the dynamic motion model. The prediction segment also obtains the predicted mean $\hat{z}(k+1|k)$ and covariance $P_{vv}(k+1|k)$ of the measurement. In the update segment, the predicted mean and covariance of $x(k+1)$ are updated using the observed measurement and the calculated Kalman gain, which is a relative weight given to the observed measurement. The UKF algorithm, for one cycle, is briefly presented below; further details can be found in [35, 36].

UKF Algorithm: Prediction

1. Denoting the sigma points with mean $\hat{x}(k|k)$ by $\chi_i(k|k)$ and their point masses by $\omega_i(k)$ at time index k, the sigma points of the prediction probability mass function (PMF) for $x(k+1)$ are computed as

$$\chi_i(k+1|k) = f[k, \chi_i(k|k), u(k)]; \quad i = -n, \ldots, n \tag{4.19}$$

2. The predicted mean $\hat{x}(k+1|k)$ and covariance $P(k+1|k)$ of $x(k+1)$ are computed as

$$\hat{x}(k+1|k) = \sum_{i=-n}^{n} \omega_i(k)\chi_i(k+1|k) \tag{4.20}$$

$$P(k+1|k) = \sum_{i=-n}^{n} \omega_i(k)[\chi_i(k+1|k) - \hat{x}(k+1|k)] \cdot [\chi_i(k+1|k) - \hat{x}(k+1|k)]^T + Q(k) \tag{4.21}$$

3. The sigma points of the prediction pmf for $z(k+1)$ are given by

$$\mathcal{Z}_i(k+1|k) = h(k, \chi_i(k+1|k)), \tag{4.22}$$

where the measurement function $h(\cdot)$ depends on the waveform transmitted. For CW, it is given by $h_{cw}()$ in (4.14), and for FM, it is given by $h_{fm}()$ in (4.17).

4. The predicted mean $\hat{z}(k+1|k)$ and covariance $P_{vv}(k+1|k)$ (also called the innovation covariance) of the observed measurement $z(k+1)$ are given by

$$\hat{z}(k+1|k) = \sum_{i=-n}^{n} \omega_i(k)\mathcal{Z}_i(k+1|k) \tag{4.23}$$

$$P_{vv}(k+1|k) = \sum_{i=-n}^{n} \omega_i(k)[\mathcal{Z}_i(k+1|k) - \hat{z}(k+1|k)] \cdot [\mathcal{Z}_i(k+1|k) - \hat{z}(k+1|k)]^T + R(k+1), \tag{4.24}$$

where $R(k+1)$ depends on the transmitted waveform. (See equations (4.15) and (4.18).)

UKF Algorithm: Update

5. The Kalman gain for the UKF is given by

$$W(k+1) = P_{xz}(k+1|k)P_{vv}^{-1}(k+1|k), \tag{4.25}$$

where P_{xz} is the cross-covariance between the predicted state and the predicted measurement. P_{xz} can be written as

$$P_{xz}(k+1|k) = \sum_{i=-n}^{n} \omega_i(k)[\chi_i(k+1|k) - \hat{x}(k+1|k)] \cdot [\mathcal{Z}_i(k+1|k) - \hat{z}(k+1|k)]^T$$

$$\tag{4.26}$$

6. The updated mean and covariance of the state $x(k+1)$ based on the observed measurement are given by

$$\hat{x}(k+1|k+1) = \hat{x}(k+1|k) + W(k+1)[z(k+1) - \hat{z}(k+1|k)] \tag{4.27}$$

$$P(k+1|k+1) = P(k+1|k) - W(k+1)P_{vv}(k+1|k)W^{-1}(k+1) \tag{4.28}$$

When clutter is present, however, multiple measurements are observed in each observation interval. In the following subsection, the probabilistic data association filter (PDAF) is discussed for extracting a single measurement from the multiple observed measurements and modifying the state error covariance update equation to account for this data association uncertainty.

4.3.4 Probability data association filter (PDAF)

Association of measurements with a target track involves two steps: defining a gating region and applying a data association filter. Establishing a validation gate around the predicted measurement within the measurement space retains the most probable measurements and
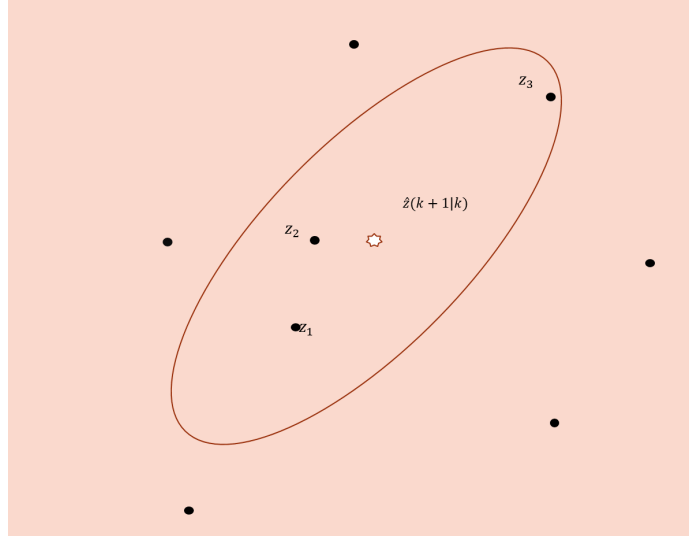
Figure 4.8: Sample instance of a validation gate in the measurement space

avoids searching for the target-associated measurement across the entire space. Figure 4.8 shows a sample instance of two-dimensional validation gate in the measurement space. The set of validated measurements are obtained by

$$\mathcal{V}(k+1,\gamma) = \{z : [z - \hat{z}(k+1|k)]'P_{vv}^{-1}(k+1|k)[z - \hat{z}(k+1|k)] \leq \gamma\}, \qquad (4.29)$$

where γ is the gate threshold corresponding to the gate probability (P_g). P_g is the probability with which the gating region is guaranteed to contain the target-generated measurement.

If the gating region has more than one measurement, the data association filter must extract (or generate) a single measurement to be associated with the target. PDAF forms a weighted measurement where each validated measurement is weighed by a corresponding association probability. The association probability for a validated observation $z_i(k)$ can be calculated as

$$\beta_i(k) = \begin{cases} \frac{e_i}{b + \sum_{j=1}^{m_k} e_j} & i = 1, ..., m_k \\ \frac{b}{b + \sum_{j=1}^{m_k} e_j} & i = 0 \end{cases}, \qquad (4.30)$$

42

where

$$e_i = \exp\{-\frac{1}{2}[z_i(k) - \hat{z}(k+1|k)]'P_{vv}^{-1}(k)[z_i(k) - \hat{z}(k+1|k)]\}, \qquad (4.31)$$

$$b = (2\pi/\gamma)^{n_z/2}m(k)/c_{n_z}(1 - \mathrm{P}_d\mathrm{P}_g)/\mathrm{P}_d, \qquad (4.32)$$

n_z is the dimension of the measurements, $m(k)$ is the total number of validated measurements, c_{n_z} is the volume of the n_z-dimensional unit radius hypersphere with $c_2 = \pi$ and $c_3 = \frac{4\pi}{3}$, and P_d is the probability of detection.

For PDAF, the modified state update equation is given by

$$\hat{x}(k+1|k+1) = \hat{x}(k+1|k) + W(k+1)\left[\sum_{i=1}^{m(k)} \beta_i(k+1)z_i(k) - \hat{z}(k+1|k)\right], \qquad (4.33)$$

and the modified state error covariance update equation with data association uncertainty is

$$P(k+1|k+1) = \beta_0(k+1)P(k+1|k) + [1 - \beta_0(k+1)]P^c(k+1|k+1) + \widetilde{P}(k+1), \qquad (4.34)$$

where the covariance update with the correct measurement $P^c(k+1|k+1)$ is given by

$$P^c(k+1|k+1) = P(k+1|k) - W(k+1)P_{vv}(k+1)W'(k+1), \qquad (4.35)$$

and the spread of innovations term $\widetilde{P}(k+1)$ is

$$\widetilde{P}(k+1) = W(k+1)\left[\sum_{i=1}^{m(k+1)} \beta_i(k+1)v_i(k+1)v_i'(k+1) - v(k+1)v'(k+1)\right]W'(k+1). \qquad (4.36)$$

43

Chapter 5: Waveform Selection Approaches and Performance Analysis

In Chapter 1, we highlighted the challenge of choosing between CW and FM pulses for tracking a target in a reverberation-limited environment. In this chapter, we address the challenge by proposing two waveform-selection approaches that can intelligently select a waveform by leveraging knowledge that CW provides additional speed information for higher Doppler targets and FM provides better range resolution for lower Doppler targets. PSBS, short for Predicted state-based selection, selects an appropriate transmission waveform based on the target's radial velocity as estimated from the predicted target state. Enhanced PSBS (EPSBS) is an enhanced version of PSBS that makes waveform selection decisions based on both predicted target Doppler and the number of gated measurements present for data association in the tracking filter. The tracking performance of the algorithms is evaluated through Monte Carlo simulations of the tracking system, consisting of the measurement data model and tracking filter modeled in the previous chapter along with the waveform selection algorithms. Performance metrics considered include position root mean square error and target in-track percentage.

This chapter is organized as follows: Section 5.1 describes the proposed predicted state-based selection (PSBS) approach and involved decision making. Section 5.2 describes the metrics used for evaluation of the tracking filter's performance; it also presents the tracking performance of the PSBS algorithm and competing waveform selection approaches for two different measurement noise scenarios and across a range of maneuver turn rates. Section 5.3 presents the EPSBS approach and its tracking performance.

5.1 Approach: Predicted State Based Selection (PSBS)

As mentioned in Section 1.2, in a reverberation-limited environment, tracking gains can be achieved by transmitting a CW waveform when the target exhibits strong Doppler and FM when it does not. The true target state, both at present and in the future, is unknown, and hence its Doppler is also unknown. However, with the help of the tracking filter, the future target state at the instant of waveform impingement can be predicted. Using the predicted state, the velocity components of the target along the line-of-sight direction (V_{los}) and in the direction orthogonal (V_{orth}) can be computed. The PSBS approach states that, if $V_{los} > V_{orth}$, indicating significant target Doppler, a CW waveform is transmitted. If not, FM is transmitted.
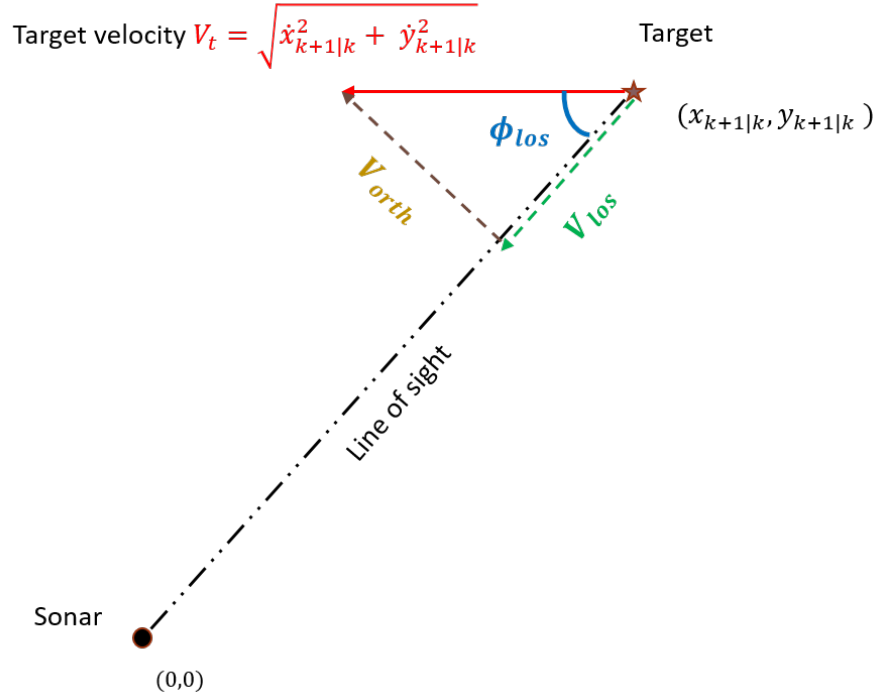
Figure 5.1: Diagram showing the locations of the target and the sonar platform. V_T is the predicted target overall velocity vector pointing in the direction of target motion, and θ_{los} is the smallest angle possible between V_T and line of sight. V_{los} is the target's predicted velocity along the line of sight, and V_{orth} is the target's predicted velocity perpendicular to the line of sight.

The predicted state is written as

$$
x(k + 1|k) = \begin{bmatrix} x_{k+1|k} \\ y_{k+1|k} \\ \dot{x}_{k+1|k} \\ \dot{y}_{k+1|k} \end{bmatrix} ,
\tag{5.1}
$$

where $(x_{k+1|k}, \; y_{k+1|k})$ represents the target's predicted position, and $\dot{x}_{k+1|k} \; \dot{y}_{k+1|k}$ represent the predicted target velocities in Cartesian coordinates. Figure 5.1 depicts the target at the predicted position with the predicted overall velocity $V_t = \sqrt{\dot{x}_{k+1|k}^2 + \dot{y}_{k+1|k}^2}$. (The sonar platform is at the origin.) The dotted line joining the target's predicted position and the origin is the line of sight (LOS) path. Vectors V_{los} and V_{orth} are the components of overall velocity vector V_t along the LOS and in the direction orthogonal to it, respectively. ϕ_{los} is the smallest angle possible between vector V_t and the LOS, as waveform choice is purely based on the magnitudes of V_{los} and V_{orth}. The minimum angle is determined as

$$
\phi_{los} = tan^{-1} \left(\frac{|m_{V_t} - m_{los}|}{1 + m_{V_t} * m_{los}} \right),
\tag{5.2}
$$

where m_{V_t} and m_{los} are the slopes of the velocity vector V_t and the LOS vector, respectively. The slopes are computed as

$$
m_{V_t} = \frac{\dot{y}_{k+1|k}}{\dot{x}_{k+1|k}} \qquad\qquad m_{los} = \frac{y_{k+1|k}}{x_{k+1|k}}.
\tag{5.3}
$$

The velocity components are determined as

$$
V_{los} = V_t cos(\phi_{los}) \qquad\qquad V_{orth} = V_t sin(\phi_{los}).
\tag{5.4}
$$

Since V_t appears in both velocity components, we compute normalized velocity components

as

$$E_{los} = \frac{V_{los}}{V_t} = cos(\phi_{los}) \qquad\qquad E_{orth} = \frac{V_{orth}}{V_t} = sin(\phi_{los}). \qquad (5.5)$$

The PSBS approach selects the transmission waveform by comparing the values of the normalized velocity components in (5.5). If $E_{los} \geq E_{orth}$ then the PSBS approach chooses a CW waveform for transmission. In contrast, if $E_{los} < E_{orth}$, then the PSBS approach chooses a FM waveform for transmission. Figure 5.2 provides a flowchart of the PSBS approach.
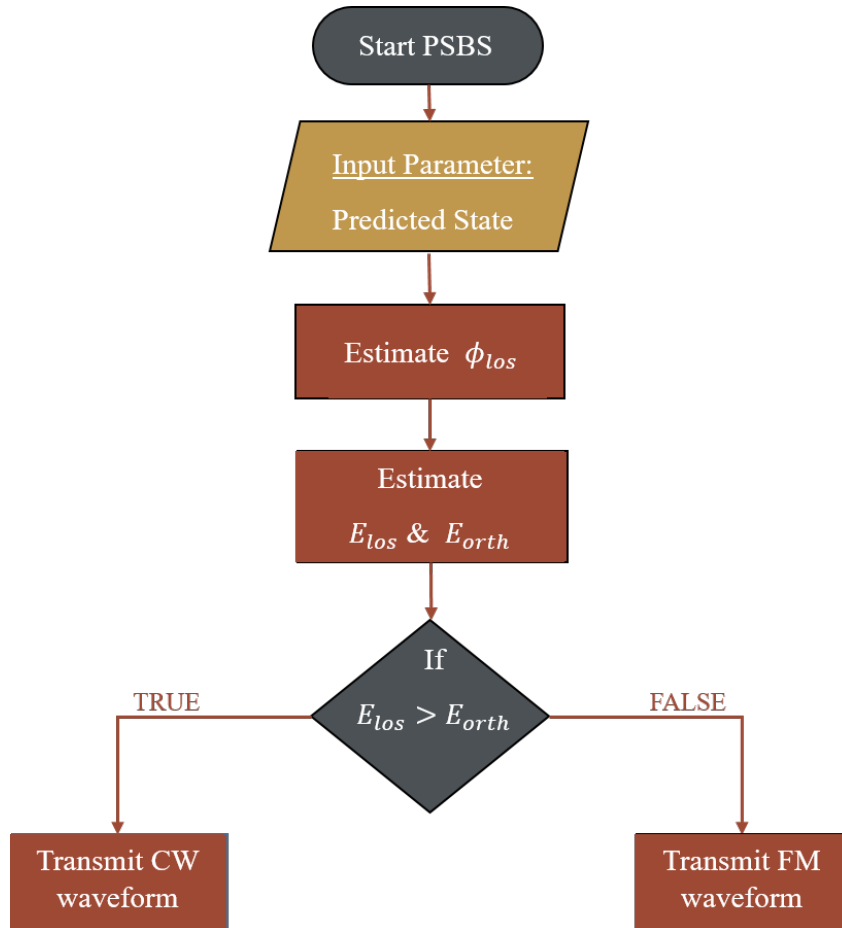
Figure 5.2: Flow chart of the PSBS waveform selection algorithm

5.2 Performance Analysis of PSBS

The performance of the PSBS approach to waveform selection is evaluated by running a set of Monte Carlo simulations of the tracking system. Figure 5.3 presents the tracking system consisting of the measurement model and tracking filter along with the PSBS algorithm, which establishes a feedback loop between the tracking filter and the measurement data model (abstraction of the sonar system behavior). The tracking performance with PSBS is compared to the performance when only FM waveforms are transmitted (All-FM) and to the performance when only CW waveforms are transmitted (All-CW).
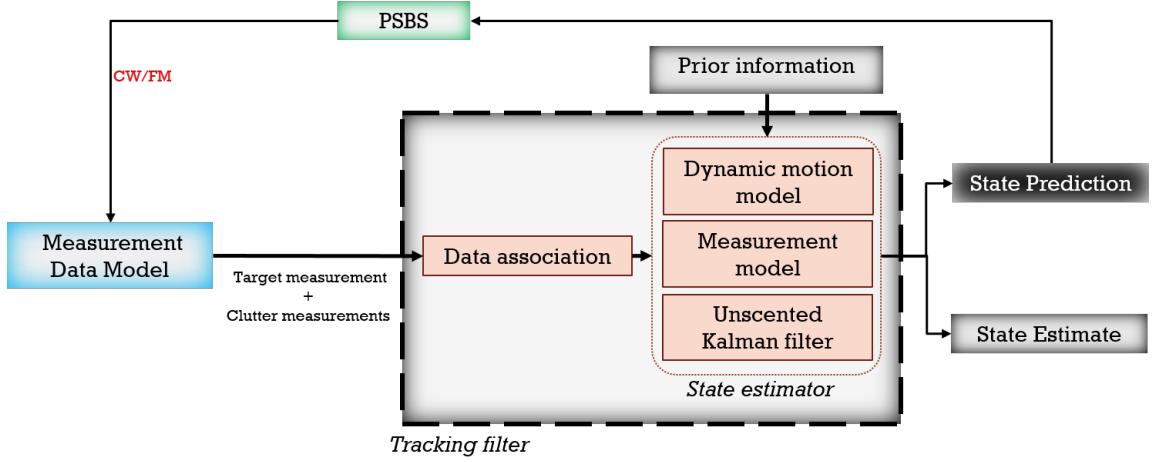
Figure 5.3: Tracking system with the PSBS algorithm

5.2.1 Performance metrics

The tracking filter estimates the state of the target at discrete time instants using measurements obtained from the measurement model. From each estimated state, the estimated location can be extracted; joining the estimated locations over time forms an estimated target path or trajectory. K denotes the set of all the estimated locations in an estimated path. In this work, target path estimation is evaluated using two metrics: Target in-track

48

percentage (TIP), and target position root mean square error (RMSE). These metrics allow us to compare tracking filter performance over different waveform selection approaches.

Target in-track percentage (TIP)

For each estimated target location in K, the distance from their corresponding true target location is computed; the distance for an estimated target location is denoted by δ. The δ for each location in set K is compared to a specified distance threshold, ε_{dist}. If $\delta < \varepsilon_{dist}$, the target is considered to be in-track and K_{IT}, a subset of K, denotes the set of estimated target locations for which target is in-track. The target in-track percentage is simply the percentage of estimated target locations in a path for which the target is in-track and can be computed as

$$\text{TIP} = \frac{\text{size}(K_{IT})}{\text{size}(K)} * 100 \tag{5.6}$$

Target position root mean square error (RMSE)

The target position RMSE captures how well the tracking filter estimates the target location. Note that the target position RMSE is computed only over the estimated target locations where the target is in-track (as defined above), as including locations where the target is not in-track would artificially inflate the RMSE value. The RMSE can be computed as

$$\text{RMSE} = \sqrt{\frac{\sum\limits_{k \in K_{IT}} \delta_k^2}{\text{size}(K_{IT})}}, \tag{5.7}$$

where δ_k is the distance between the estimated position k, for which target is in-track, and the corresponding true target position.

5.2.2 PSBS performance results

The performance of the PSBS approach and of single-waveform approaches is simulated for target turn rates ranging from 1°/sec to 8.5°/sec and two levels of measurement noise. Table 5.1 presents two versions of measurement noise used in generating the measurement data. In each noise version, σ_{Range} for CW is chosen to be a multiple of σ_{Range} for FM, as the measured range accuracy is dependent on the bandwidth of the transmitted signal and is better for FM (discussed in Subsection 2.3.1). σ_{Bearing} is the same for both waveforms as the bearing accuracy is independent of the transmitted waveform. $\sigma_{\text{RangeRate}}$ exists only for CW, as we assume that the transmission of FM does not allow us to estimate range-rate. The noise versions differ from one another only in terms of the noise induced in the range dimension; noise version V_2 induces higher noise in the range data produced by the measurement data model.

Table 5.1: Two versions of measurement noise

(a) Measurement noise version V_1

	CW	**FM**
$\boldsymbol{\sigma}_{\text{Range}}$	$40m$	$10m$
$\boldsymbol{\sigma}_{\text{Bearing}}$	1°	1°
$\boldsymbol{\sigma}_{\text{RangeRate}}$	$0.5m/sec$	-

(b) Measurement noise version V_2

	CW	**FM**
$\boldsymbol{\sigma}_{\text{Range}}$	$75m$	$25m$
$\boldsymbol{\sigma}_{\text{Bearing}}$	1°	1°
$\boldsymbol{\sigma}_{\text{RangeRate}}$	$0.5m/sec$	-

For each combination of measurement noise level and turn rate, 3000 Monte Carlo simulations are performed, i.e., 3000 target trajectories are generated. Each trajectory, simulated for a maximum period of 400 seconds, starts from location (6000,4000) in Cartesian coordinates and is contained in a surveillance region limited to a radial distance of 7500 meters from the origin (the location of the sonar platform). With sound pulses assumed to be transmitted every 2 seconds, based on the simulated path and the transmitted sound pulse, the measurement data model generates measurement data spaced 2 seconds apart. The measurement data points are input to the tracking filter for target path estimation.

To estimate the simulated path, the tracking filter is initialized with an updated target state estimate at time instant 0, $\hat{x}(0|0)$, as

$$\hat{x}(0|0) = \begin{bmatrix} \hat{x}_{0|0} \\ \hat{y}_{0|0} \\ \hat{\dot{x}}_{0|0} \\ \hat{\dot{y}}_{0|0} \end{bmatrix} = \begin{bmatrix} 6000 \\ 4000 \\ -24.96 \\ -16.64 \end{bmatrix},$$

and an updated target state covariance at time instant 0, $P(0|0) = 10I_4$, where I_n denotes the $n \times n$ identity matrix. The quantities $\hat{x}(0|0)$ and $P(0|0)$ are used to predict the target state for the first ping instant, i.e., to compute $\hat{x}(1|0)$, which is input to the PSBS algorithm for determining the transmitted waveform. Based on the waveform chosen, the measurement data model generates appropriate target and clutter measurements which are input to the tracking filter for the predicted state update. In the tracking filter, the measurement data is processed by the PDAF and the predicted state is updated. For data association, the gate threshold is set to $\gamma = 16$, the probability of detection is $P_d = 1$, and the gate probability is $P_g = 0.99$. The above procedure is repeated for all the ping instants in the simulated path, and an estimated target trajectory is obtained from the estimated sates. Similarly, for the same simulated path, the target trajectory is estimated by tracking filter with All-CW and All-FM approaches for comparison. Figure 5.4 shows a simulated target path in a Monte Carlo simulation and the paths estimated by the tracking filter with different waveform selection approaches.

The performance of the tracking filter with a waveform selection strategy is obtained by evaluating the chosen performance metrics, TIP and RMSE, for each simulated trajectory and averaging over the 3000 simulations. In evaluating TIP, the distance threshold (ϵ_{dist}) is set to 250 m. Figures 5.5 and 5.6 plots the performance metrics evaluated for all the waveform selection approaches for measurement noise scenario V_1 and turn rates ranging from 1°/sec to 8.5°/sec. Similarly, Figures 5.7 and 5.8 display simulated performance results
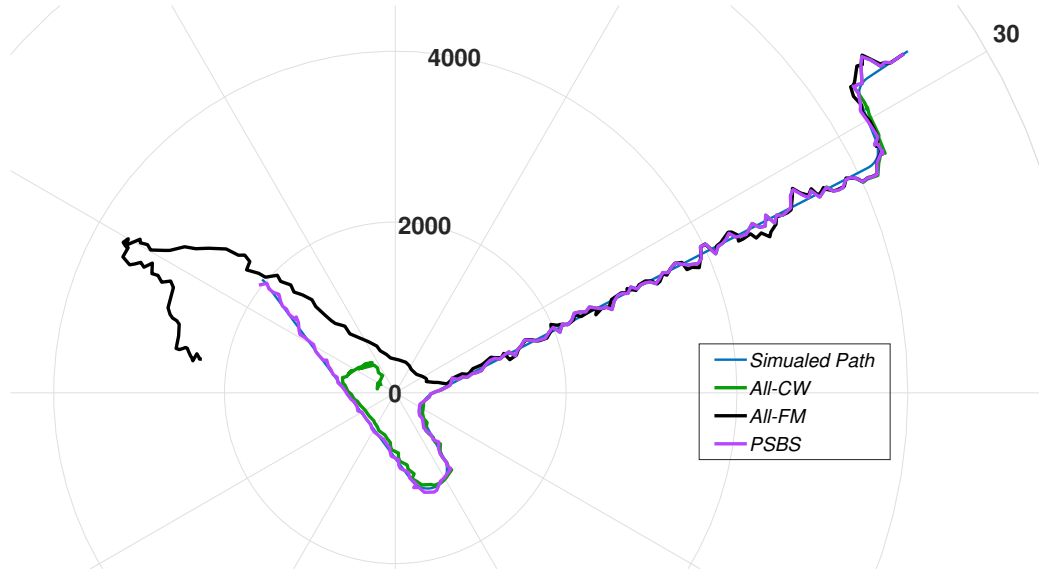
(a) Simulated path and the paths estimated by tracking filter using different waveform selection approaches
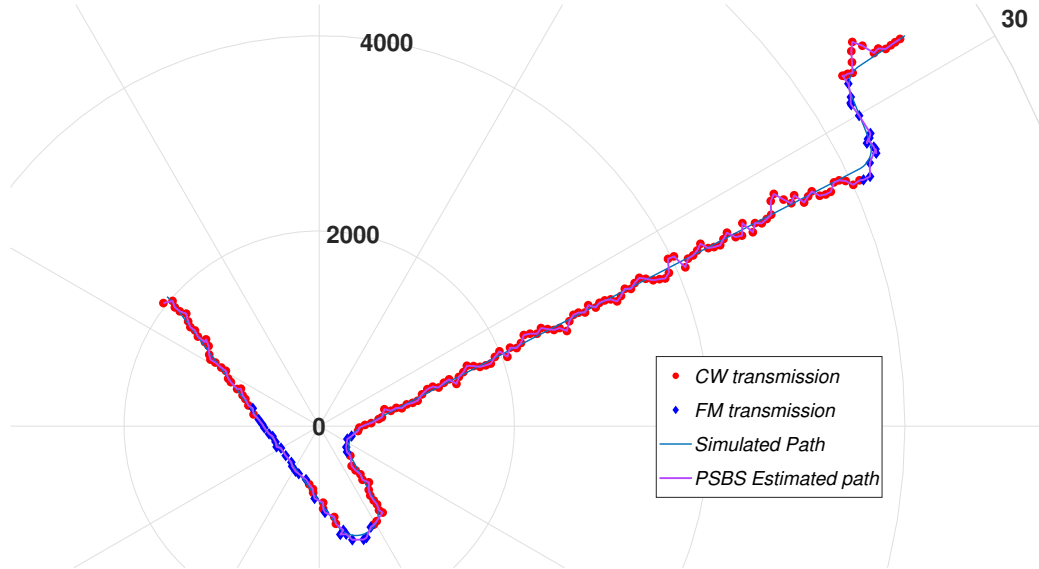
(b) Path estimated by the tracking filter using PSBS and the waveform choice at each ping instant

Figure 5.4: (a) Simulated target path for a target turn-rate of 7.5°/sec and the paths estimated by the PSBS, All-CW, and All-FM wave selection approaches. All-CW and All-FM have difficulty tracking the target through the end of the path whereas PSBS tracks the target closely throughout. (b) PSBS-estimated target path along with the waveform choices made by the PSBS algorithm at different ping instants. Since the target direction changes gradually, the PSBS approach often tends to choose the same waveform for several subsequent ping instants.

for measurement noise scenario V_2. Tables of the plotted performance metric data are provided in Appendix A.

5.2.3 Discussion of performance results

From Figures 5.5 and 5.7, it is clear that across both levels of measurement noise, the PSBS approach produces the smallest target position RMSE when compared to the All-CW and All-FM approaches. Selecting the transmitted waveform based on the predicted target state generated by the tracking filter yields improved accuracy in the estimated target location. It is also evident from the performance plots that the PSBS approach yields the largest reduction in target position RMSE at turn rates for which the All-CW and All-FM approaches perform similarly in terms of position RMSE.

From Figures 5.6 and 5.8, we see that apart for turn-rates from 1°/sec to 3°/sec, the TIP for the PSBS approach is largest when compared to the All-CW and All-FM approaches. For turn rates of 3°/sec and above, selecting the transmitted waveform based on the predicted target state generated by the tracking filter improves the tracker's ability to maintain the target track. From Figure 5.6, it is evident that the TIP improvement shown by the PSBS approach is maximized at turn-rates from 4.5°/sec to 6°/sec, where the performance of All-CW is similar to that of All-FM. Similarly, in Figure 5.8, more improvement can be observed between the turn-rates 3.5°/sec to 6.5°/sec. From figures 5.6 and 5.8, it is observable that the TIP of PSBS approach stays nearly flat till the turn-rates 6°/sec and 4.5°/sec respectively, even though the TIP of All-CW and All-FM seems to decrease linearly with the turn-rate.

From the above results and discussion, we see that the PSBS approach gives improved target tracking relative to choosing a single waveform to transmit throughout the tracking process. However, the simulation results also reveal potential shortcomings of the PSBS approach. First, for both measurement noise scenarios, the All-CW approach yields the largest TIP (better than the PSBS approach) when the turn rate is very low. A likely explanation is that at low turn rates, the All-CW tracking in-track percentage is nearly 100%, so there is little opportunity for improvement through intelligent waveform selection.

Figure 5.5: Target position root mean square error (RMSE) as a function of turn-rate for measurement noise scenario V_1

Figure 5.6: Target in-track percentage (TIP) as a function of turn-rate for measurement noise scenario V_1
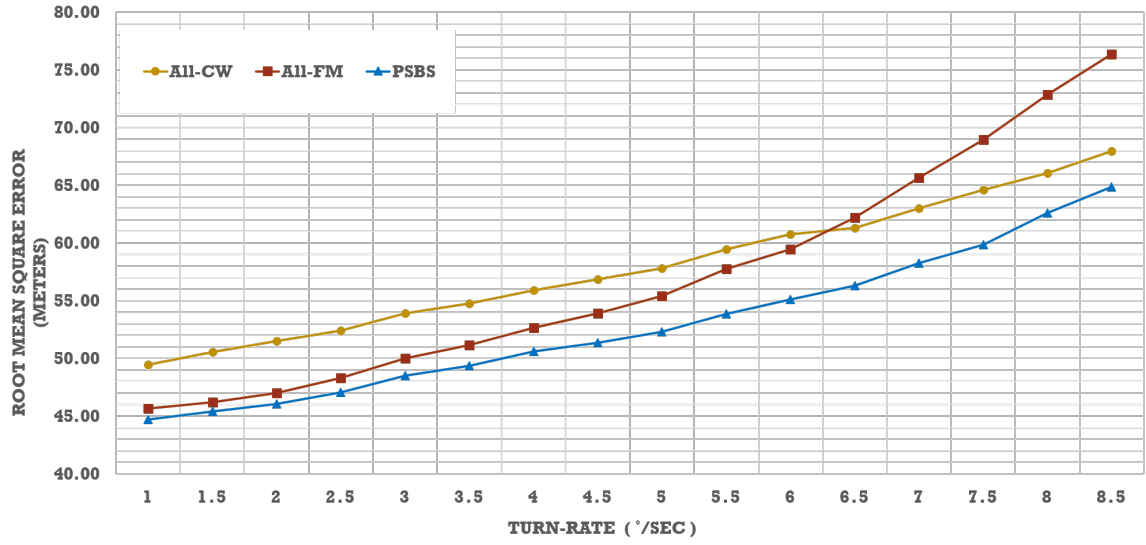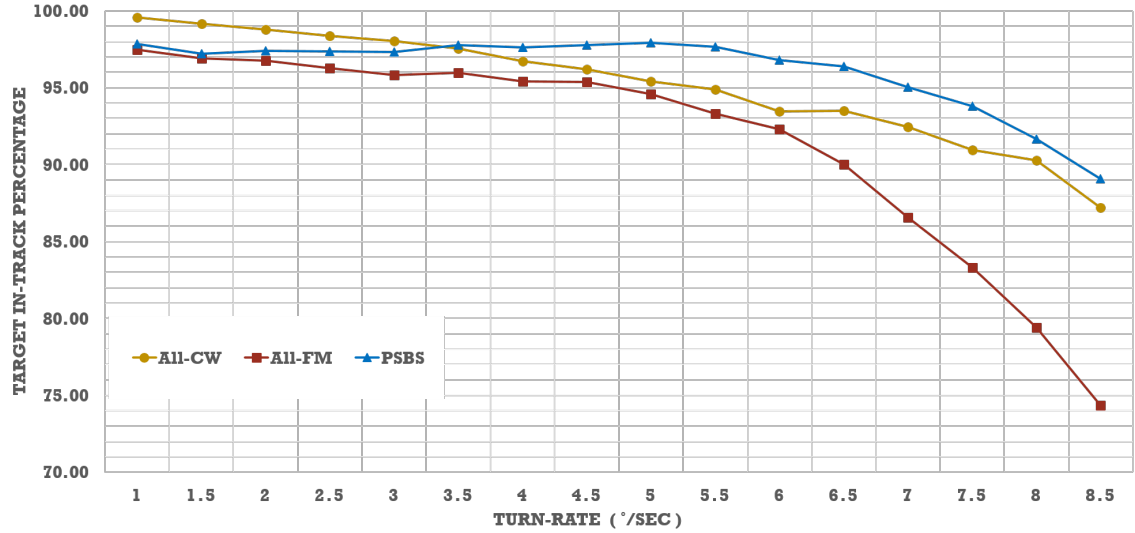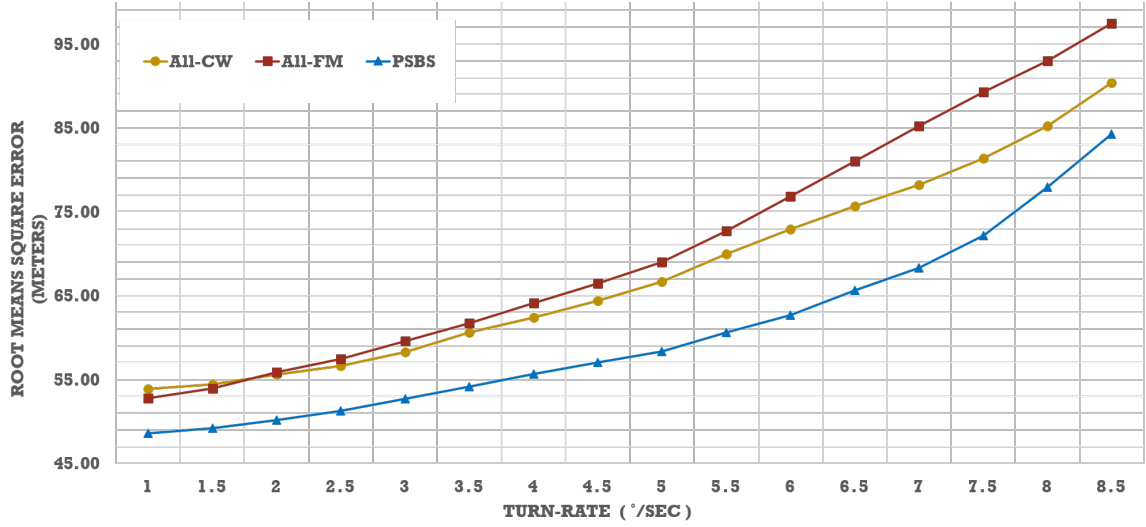
Figure 5.7: Target position root mean square error (RMSE) as a function of turn-rate for measurement noise scenario V_2
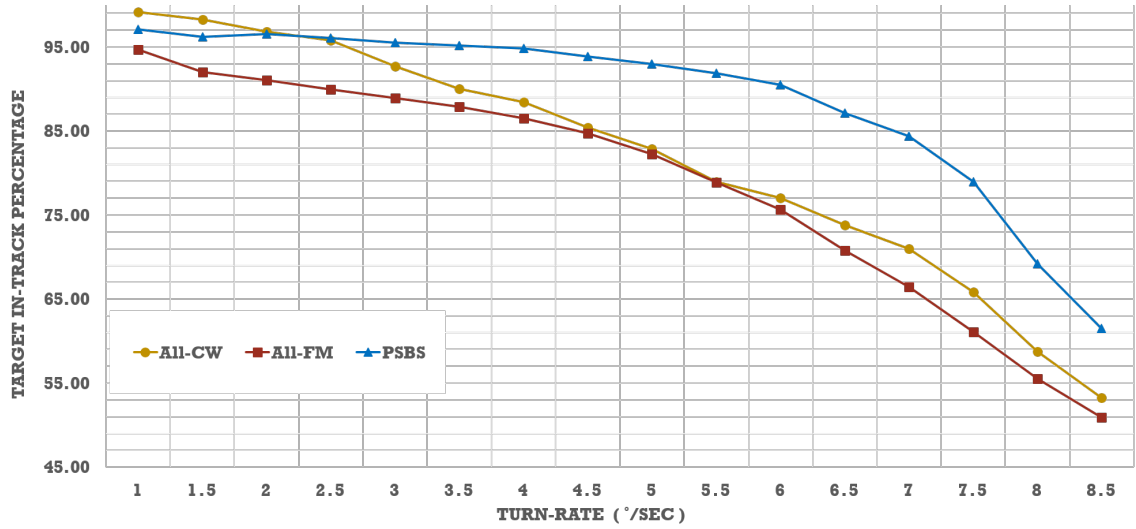
Figure 5.8: Target in-track percentage (TIP) as a function of turn-rate for measurement noise scenario V_2

In the RMSE and TIP plots for both measurement noise scenarios, we see that as the turn rate increases from its lowest value to 6°/sec, the performance metric plots are nearly linear. Beyond the turn-rate 6.5°/sec, the performance for the All-FM approach worsens rapidly, no longer changing linearly. The second shortcoming of the PSBS approach is that its performance follows that of the All-FM approach at higher turn rates even though the All-CW approach exhibits relatively stable performance. As discussed and shown in Figure 5.4b, PSBS tends to choose the same waveform for several adjacent pings instants. When PSBS chooses FM waveform for several adjacent pings, the PSBS suffers from the same phenomenon (discussed in detail later) that is responsible for track loss in All-FM approach. Thus, the performance of PSBS follows the All-FM performance at higher turn-rates. This shortcoming can be addressed by enhancing the PSBS approach to choose CW waveform when performance degradation is sensed with FM waveform transmissions. The phenomenon responsible for performance degradation and the enhanced PSBS approach are discussed in the next section.

5.3   Enhanced Predicted State Based Selection (EPSBS)

As discussed above, the performance of the PSBS waveform selection approach degrades at high turn rates, following the poor performance of the All-FM approach. Understanding the process responsible for performance degradation in the All-FM approach at higher turn rates helps in devising modifications to the PSBS approach to improve high turn-rate performance. One element that can degrade tracking performance is an error in data association. In particular, a single incorrect (clutter) measurement may receive a high probability (weight), or there may be a large number of measurements inside the validation gate, each assigned a small association weight.

In PDAF, each measurement is assigned an association weight proportional to its distance from the predicted target location. With many measurements in the gate, each measurement is often assigned a small probability, resulting in inaccurate state estimation

and larger updated state covariance. Larger updated state covariance leads to a larger gate in the next cycle and hence a larger number of measurements within the gate. This process can be cumulative, leading to loss of target track. The number of measurements inside the validation gate can be considered as an indicator of this issue and used as a cue to take modified action in waveform selection.
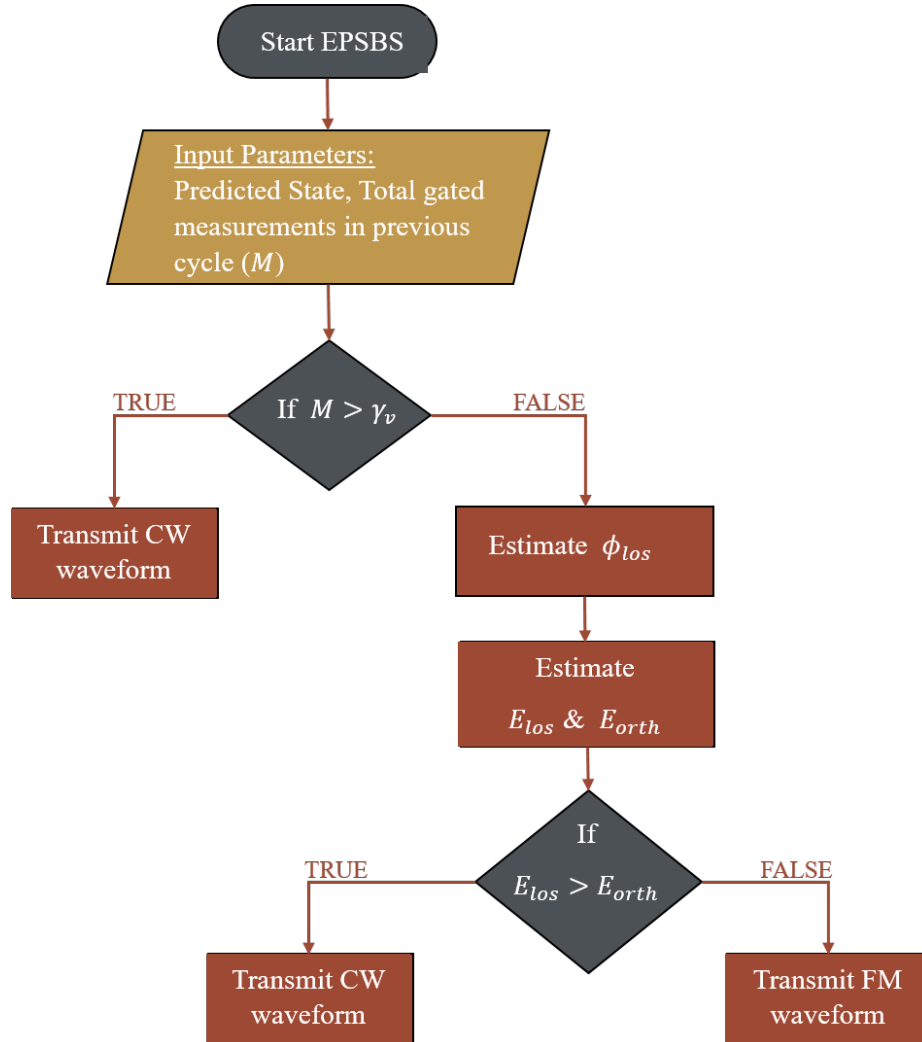
Figure 5.9: Flowchart of EPSBS

The increasing number of measurements within the validation gate is a situation that

occurs almost exclusively when a series of FM waveforms are transmitted. In contrast, when a CW waveform is transmitted, the resulting measurements are three-dimensional, and the validation gate is an ellipsoid. The inclusion of a third dimension (range rate) allows the validation gate to filter out more clutter measurements, mitigating the challenge of having a large number of measurements within the gate. This benefit of CW transmission is the motivation behind the proposed enhancement to the PSBS approach.

To address the issue of growing numbers of measurements in the validation gate, we modify PSBS to select a CW waveform for transmission when the number of measurements in the gate exceeds a pre-defined threshold, regardless of the predicted target velocity. Figure 5.9 provides a flowchart of the enhanced PSBS (EPSBS) algorithm. The threshold on the number of validated measurements is denoted by (γ_v); if the number of gated measurements (M) in the previous cycle (ping) is greater than γ_v, then a CW waveform is transmitted. If $M < \gamma_v$, the PSBS algorithm operates in its standard form, choosing the transmitted waveform based on the predicted target velocity.

5.3.1 Performance analysis of EPSBS

As with PSBS, the performance of the EPSBS approach was evaluated by running a set of Monte Carlo simulations of the tracking system with the EPSBS waveform selection approach, which establishes the feedback loop between the tracking filter and measurement model. The performance of EPSBS is compared to that of All-CW, All-FM, and PSBS for turn rates from 1°/sec to 8.5°/sec and for the two measurement noise scenarios V_1 and V_2. For each combination of measurement noise and turn rate, 3000 Monte Carlo simulations were performed. All parameters related to target path simulation and tracking filter are the same as given in Section 5.2.2. In EPSBS, the threshold on the number of measurements in the gate is set to $\gamma_v = 7$ based on heuristic observation. Figure 5.10 presents a simulated path in a Monte Carlo simulation and the paths estimated by tracking filter using EPSBS and other wave selection approaches. Figure 5.11 shows the paths estimated when using the PSBS and EPSBS approaches along with the waveforms chosen by corresponding approaches

58
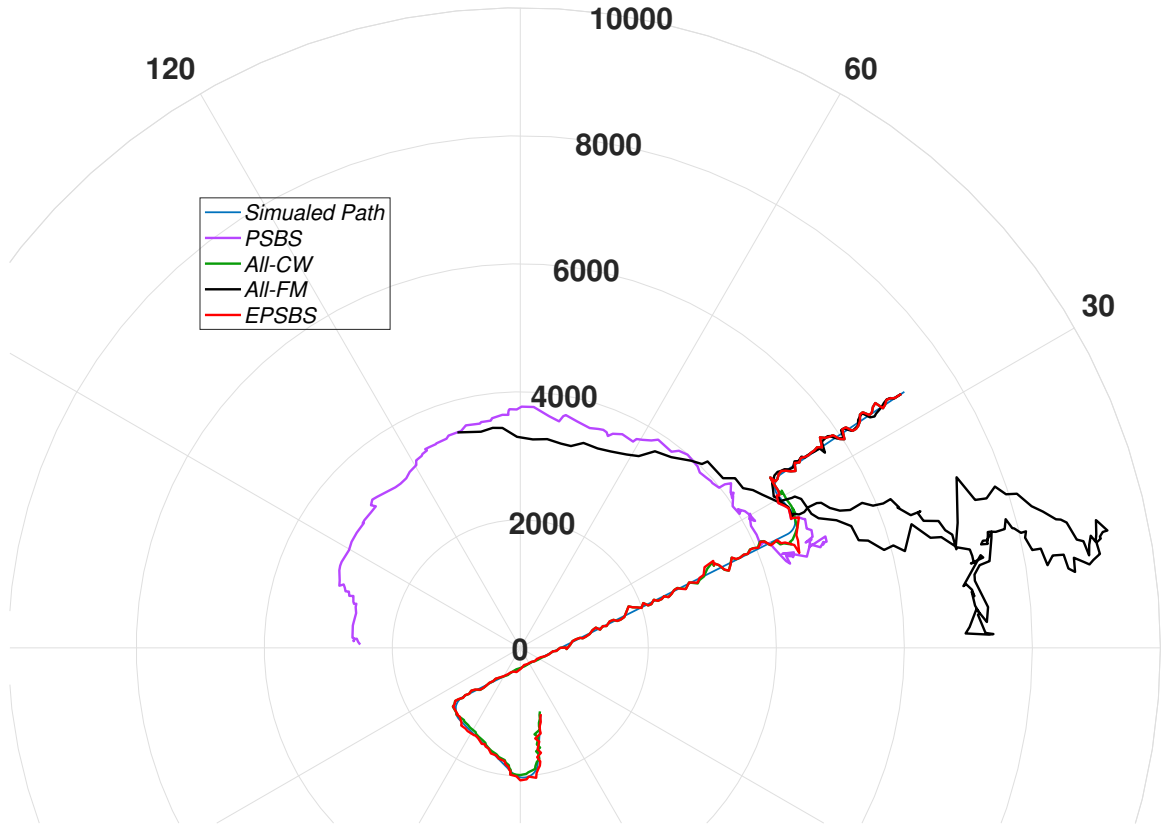
Figure 5.10: Simulated path and estimated paths by the tracking filter using EPSBS, PSBS, All-CW, and All-FM approaches. In this particular realization, the target path is simulated for a target turn-rate of 7.5°/sec. Only the EPSBS and All-CW approaches can track the target through the end of the simulated trajectory; the All-FM and PSBS approaches lose the target track while the target is performing the second maneuver. This realization is a sample instance where All-FM suffers from the track loss due to the data association error from the presence of a larger number of measurements inside the validation gate. As the PSBS chooses waveform based only on the predicted target velocity, it chooses FM waveform for several adjacent pings on the path segment between first and second maneuver (shown in figure 5.11a). Thus, the PSBS suffers the same fate as the All-FM approach. On the other hand, EPSBS tracks the target through the end, similar to All-CW, as it makes a decision based on predicted target velocity and the number of gated measurements in the previous cycle. More comparisons between the EPSBS waveform decisions and PSBS waveform decisions are presented in Figure 5.11
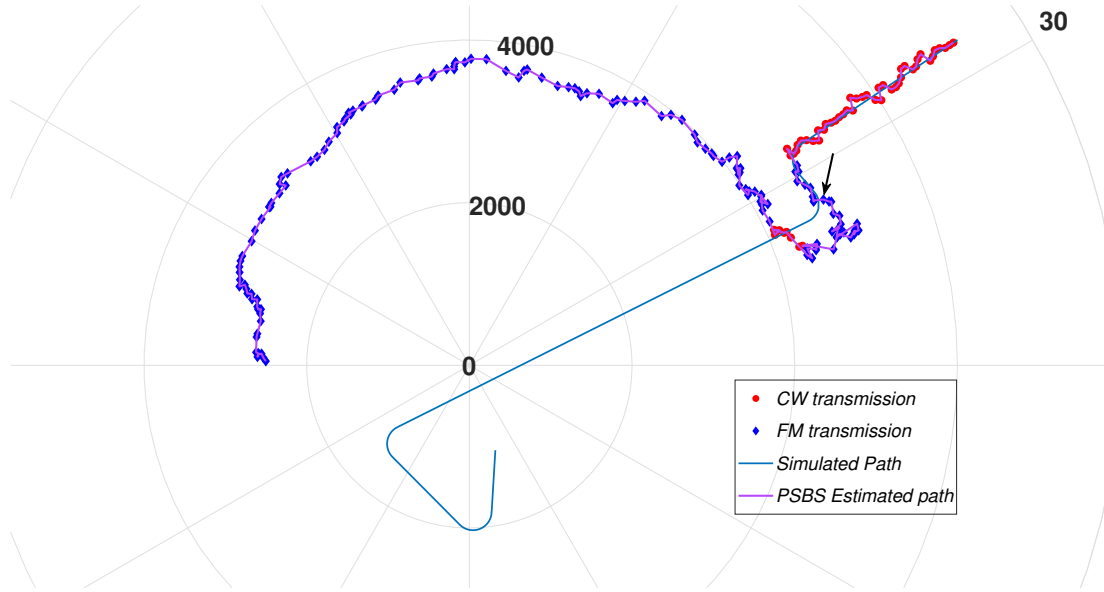
(a) Simulated path and the path estimated by the PSBS approach along with the chosen waveform at each ping instant.
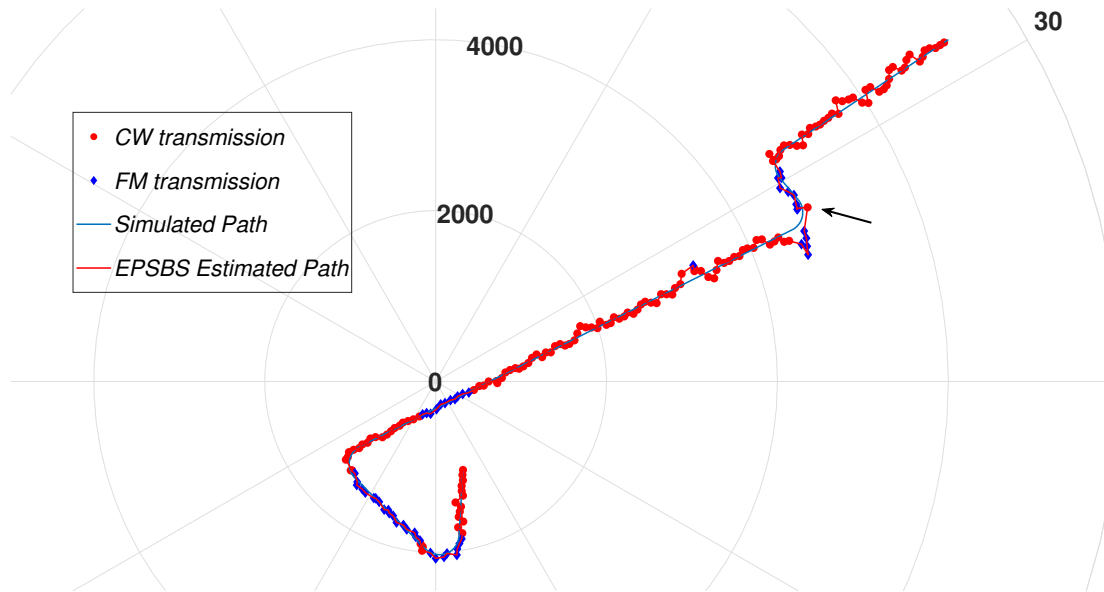
(b) Simulated path and the path estimated by the EPSBS approach along with the chosen waveform at each ping instant.

Figure 5.11: Plots in (a) and (b) are alike until the ping indicated by the arrow. At this ping instant, in plot (a) the PSBS chose FM based on the predicted target velocity, and the subsequent estimated states veered off of the simulated path. In plot (b), the EPSBS considered the total number of gated measurements (greater than γ_v) and chose CW instead of FM, allowing the estimated path to follow the simulated path closely without losing the target.

at each ping instant.

Figures 5.12 and 5.13 show the target position RMSE and TIP values as a function of turn rate for measurement noise scenario V_1. Similarly, Figures 5.14 and 5.15 show the target position RMSE and TIP values as a function of turn rate for measurement noise scenario V_2. The average performance of EPSBS and other approaches in terms of TIP and RMSE is displayed in table form in Appendix B.

At higher turn rates, the performance of the PSBS approach degrades as turn rate increases, similar to All-FM approach. From Figures 5.12, 5.13, 5.14 and 5.15 it is clear that EPSBS is able to address this issue and enhance tracking performance with respect to both metrics. At high turn rates, the EPSBS achieves performance that is nearly linear like that of the All-CW approach.

From Figures 5.12 and 5.14, it is clear that, for both versions of observation noise, EPSBS has lower position RMSE compared to all other approaches for turn rates above 5°/sec and equivalent RMSE for lower turn rates. Hence, selecting the transmitted waveform based on the number of gated measurements in the previous cycle and the target predicted state maintains the RMSE benefits of the PSBS approach at lower turn rates and delivers even better RMSE performance at higher turn rates.

From Figures 5.13 and 5.15, for both versions of observation noise, the TIP achieved using EPSBS is almost identical to the TIP achieved using PSBS for turn rates up to 5.5°/sec. For turn rates larger than 5.5°/sec, EPSBS delivers a larger TIP than PSBS. Hence, for turn rates of 5.5°/sec and below, waveform selection based on only predicted state, or both predicted state and number of gated measurements, gives the same tracking filter accuracy. For turn-rates beyond 5.5°/sec, the additional decision factor of the number of gated measurements improves tracking filter accuracy. Note, however, that for noise version V_2 at a turn-rate of 5.5°/sec, the TIP of EPSBS is slightly lower than that of the PSBS approach (see Figure 5.15). This suggests that when All-CW and All-FM achieve nearly identical TIP, it is preferable to choose the transmitted waveform based on the predicted target velocity. However, this demands further research on whether this suggestion can
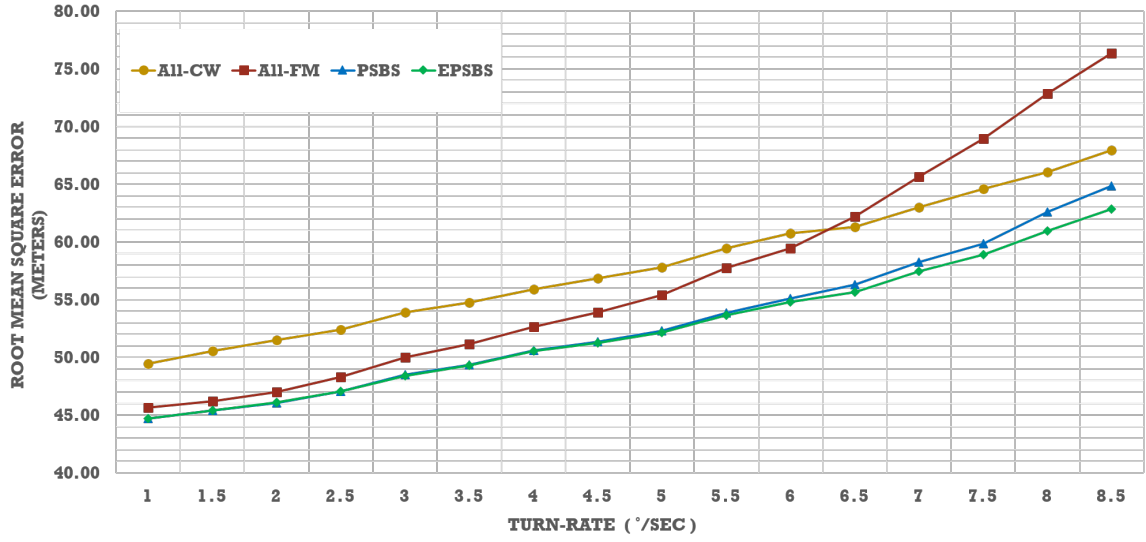
Figure 5.12: Target position root mean square error (RMSE) as a function of turn-rate for measurement noise scenario V_1
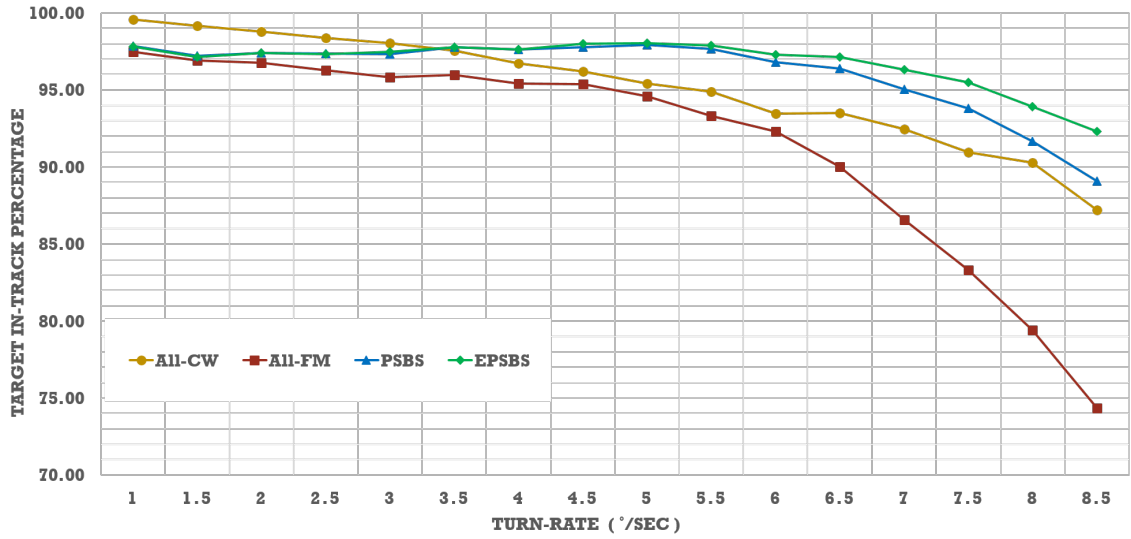
Figure 5.13: Target in-track percentage (TIP) as a function of turn-rate for measurement noise scenario V_1
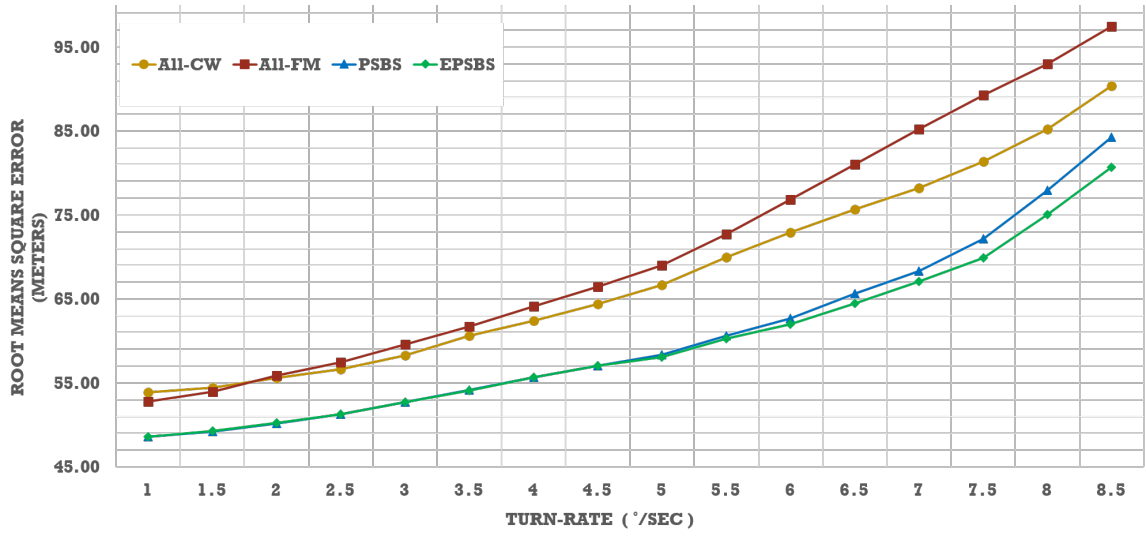
Figure 5.14: Target position root mean square error (RMSE) as a function of turn-rate for measurement noise scenario V_2
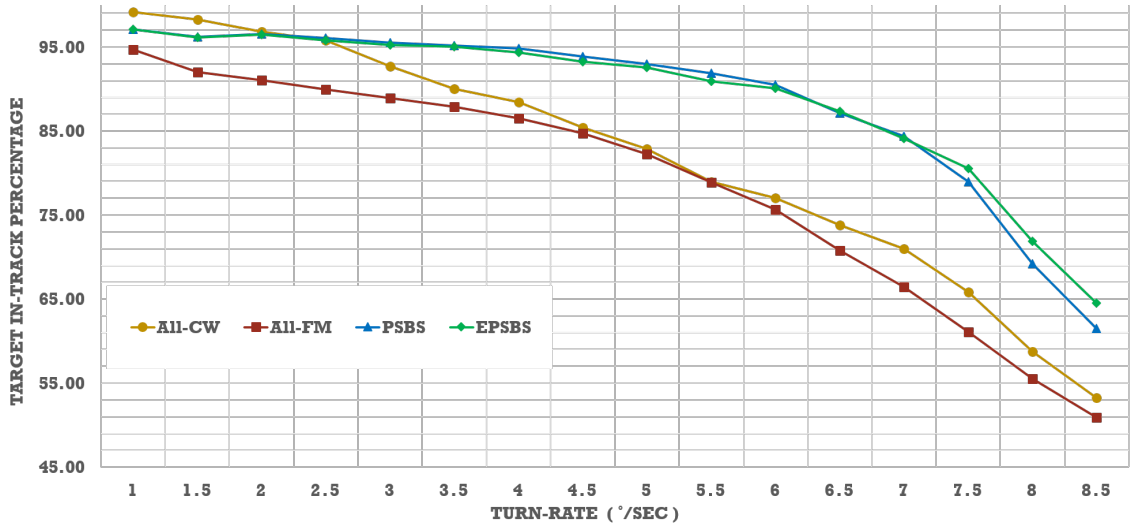
Figure 5.15: Target in-track percentage (TIP) as a function of turn-rate for measurement noise scenario V_2

be generalized to all the cases, and why looking at the number of gated measurements is hurting the TIP of EPSBS?

Chapter 6: Conclusions

6.1 Summary

Tracking an underwater target with active sonar involves transmitting a sound pulse in water and listening for the echo from the target. CW and FM are common waveforms in active sonar. CW pulses allow for measurement of target Doppler (range-rate) but have relatively poor range resolution, whereas FM pulses are relatively insensitive to Doppler but have better range resolution. In a reverberation-limited environment, a fine range resolution is required to separate and track a low Doppler target from clutter, whereas, in the case of high Doppler target, extraction of Doppler information is required. It is clear from the above discussion that neither of the standard waveforms can achieve the goals of fine range resolution and Doppler shift extraction simultaneously. The complementary nature of the waveforms discourages us from using one of the pulses for all the scenarios and necessitates the intelligent selection of waveform at each ping, using target Doppler information, for improved target tracking. However, the target's Doppler is not known at the time of waveform transmission and changes over time. This uncertainty raises the question that motivated the research: How can the system select between the two waveforms to maximize tracking capability?

Prior approaches had been developed to select transmission waveforms in both adaptive and non-adaptive ways. The adaptive approaches select the waveform that minimizes a cost function that is an indicator of the overall tracking system performance; it results in a feedback loop between the tracking filter and the transmitter. This thesis, however, investigated the possibility of adaptive waveform selection based on characteristics of the target and the environment for better tracking performance; it proposed the PSBS and EPSBS algorithms, where PSBS uses the estimated range-rate of the target, and EPSBS

65

uses both the target range-rate etimate and the number of clutter measurements inside the validation gate. Both algorithms establish a feedback loop between the measurement model and the tracking filter.

We set up a platform for PSBS and EPSBS algorithm evaluation by developing a tracking system model consisting of a target path simulator, measurement data model, and tracking filter. The performance of the PSBS and EPSBS algorithms was evaluated in terms of TIP and RMSE by conducting 3000 Monte Carlo simulations on the tracking system with the corresponding wave selection algorithm, for all the combinations of target turn-rates ranging from 1°/sec to 8.5°/sec and two levels of measurement noise. The performance was compared to that of transmitting either CW always (All-CW) or FM always (All-FM). From the PSBS performance evaluation, it is evident that choosing the transmitted waveform based on the predicted state gives improved tracking performance relative to choosing a single waveform to transmit throughout the tracking process. The PSBS algorithm improved the target localization estimates by 7.7% on average from the next best performing approach, over all the turn-rates, with the largest improvement being 14%. The PSBS also improved the target in-track percentage by 5.5% on average from next best performing approach, over all the turn-rates, with the largest improvement being 20%.

While PSBS improves significantly upon All-CW or All-FM, It suffers substantial performance degradation for highly maneuvering targets, similar to All-FM approach, even though the All-CW approach exhibits relative stable performance. The All-FM approach poor performance at the higher turn-rates is mainly because of the error in the data association with the presence of a large number of measurements inside the validation gate. We addressed this shortcoming by suggesting an enhancement to the PSBS approach: Enhanced PSBS (EPSBS). Along with the predicted state, EPSBS takes into account the number of validated measurements in the previous cycle when making the waveform decision. Simulation results show that EPSBS eliminates the performance degradation observed for PSBS when target undergo rapid maneuvers. The EPSBS algorithm improved the target localization estimates by 8.5% on average from the best performing approach between

All-CW and All-FM, over all the turn-rates, with the largest improvement being 15%. The EPSBS also improved the target in-track percentage by 6.1% on average, from the best performing approach between All-CW and All-FM, over all the turn-rates, with the largest improvement being 22.4%.

From the results obtained in this thesis, we can conclude that the intelligent selection of transmitted waveform can significantly improve tracking performance in active sonar. However, the proposed algorithms do have some limitations. Both algorithms, for turn-rates below 3°/sec, do not perform better than the All-CW approach in terms of target in-track percentage. A likely explanation is that at low turn rates, the All-CW target in-track percentage is nearly 100%, so there is little scope left for improvement through PSBS and EPSBS. The second limitation is that the performance of PSBS is heavily impacted if one of the waveform options performs poorly. In the situation of an FM waveform performing far worse than a CW waveform, the Enhanced PSBS can reduce the effect of poor FM performance.

6.2   Suggestions for Further Research

The existing literature on adaptive waveform selection is focused on choosing an optimal waveform that minimizes a cost function. This thesis opens up a new direction by making waveform decisions based on the target characteristics and the environment. This research also aids in developing intelligent waveform selection mechanisms for cognitive sonar. The work in this thesis focuses on a single target and one-step-ahead prediction; this can be easily extended to multiple-step-ahead prediction and multiple target cases.

In this thesis, we used the Unscented Kalman filter with a single dynamic motion model abstracting straight line and maneuver motions of the target. The behavior of the intelligent waveform selection can be further examined by adopting more complex tracking filters, such as the Interactive Multiple Model (IMM) filter with a dynamic model for each type of motion exhibited by the target. Another area of possible research is testing the algorithms with a complex model of an active sonar system. In this work, we abstracted the system

using a simple measurement data model block. However, a complex model that involves better modeling of transmitted and received signals, and interactions with the environment can be used to further investigate the applicability of the algorithms to real-world situations. Finally, future research can also be focused on extending the algorithms to address additional system parameters such as ping rate, beam steering, and detection threshold.

Appendix A: PSBS Performance Comparison Tables

In this appendix, the performance comparison tables, presenting the performance metrics, for the All-CW, All-FM, and PSBS approaches, for turn rates ranging from 1°/sec to 8.5°/sec and for measurement noise scenarios V_1 and V_2, are presented. The performance shown in the comparison tables is the averaged performance over 3000 Monte Carlo simulations. The data related to the figures 5.5 and 5.6 displayed in chapter 5 are presented in table A.1. Similarly, the data related to the figures 5.7 and 5.8 displayed in chapter 5 are presented in table A.2.

Each performance comparison table is subdivided into three sub-tables: (a), (b), and (c). Sub-table (a) presents a version of measurement noise, in terms of standard deviation (σ) of a zero-mean Gaussian noise in their corresponding dimensions, used in the generation of CW and FM versions of target-generated measurements in the measurement data. Sub-table (b) shows the averaged tracking filter performance, in terms of target position root mean square error, with All-CW, All-FM, and PSBS approaches, for turn-rates ranging from 1°/sec to 8.5°/sec. Sub-table (c) shows the averaged tracking filter performance, in terms of target in-track percentage, with All-CW, All-FM, and PSBS approaches, for turn-rates ranging from 1°/sec to 8.5°/sec.

Table A.1: PSBS performance comparison table for measurement noise version V_1

(a) Measurement noise version V_1

	CW	FM
$\boldsymbol{\sigma}_{\text{Range}}$	40m	10m
$\boldsymbol{\sigma}_{\text{Bearing}}$	1°	1°
$\boldsymbol{\sigma}_{\text{RangeRate}}$	0.5m/sec	-

(b) Target position root mean square error (in Meters) for a range of turn rates

Turn-Rate	1	1.5	2	2.5	3	3.5	4	4.5
All-CW	49.43	50.56	51.48	52.42	53.90	54.73	55.92	56.82
All-FM	45.67	46.18	46.97	48.31	50.01	51.17	52.65	53.88
PSBS	44.70	45.40	46.07	47.05	48.48	49.35	50.61	51.37

Turn-Rate	5	5.5	6	6.5	7	7.5	8	8.5
All-CW	57.81	59.45	60.73	61.30	62.99	64.57	66.04	67.95
All-FM	55.41	57.75	59.47	62.18	65.65	68.93	72.83	76.35
PSBS	52.31	53.84	55.11	56.28	58.25	59.85	62.60	64.83

(c) Target in-track percentage for a range of turn rates

Turn-Rate	1	1.5	2	2.5	3	3.5	4	4.5
All-CW	99.57	99.17	98.80	98.36	98.02	97.54	96.72	96.19
All-FM	97.49	96.93	96.77	96.26	95.84	95.98	95.41	95.36
PSBS	97.84	97.20	97.42	97.38	97.31	97.76	97.62	97.78

Turn-Rate	5	5.5	6	6.5	7	7.5	8	8.5
All-CW	95.42	94.89	93.48	93.51	92.44	90.96	90.28	87.21
All-FM	94.58	93.32	92.30	90.00	86.57	83.29	79.42	74.36
PSBS	97.94	97.65	96.81	96.39	95.04	93.79	91.67	89.07

Table A.2: PSBS performance comparison table for measurement noise version noise V_2

(a) Measurement noise version V_2

	CW	FM
σ_{Range}	75m	25m
σ_{Bearing}	1°	1°
$\sigma_{\text{RangeRate}}$	0.5m/sec	-

(b) Target position root mean square error (in Meters) for a range of turn rates

Turn-Rate	1	1.5	2	2.5	3	3.5	4	4.5
All-CW	53.89	54.40	55.61	56.60	58.24	60.61	62.40	64.39
All-FM	52.80	53.97	55.89	57.46	59.54	61.73	64.11	66.46
PSBS	48.56	49.21	50.19	51.28	52.72	54.14	55.64	57.04

Turn-Rate	5	5.5	6	6.5	7	7.5	8	8.5
All-CW	66.67	69.91	72.87	75.66	78.17	81.35	85.22	90.36
All-FM	68.98	72.69	76.81	80.99	85.23	89.27	92.95	97.45
PSBS	58.32	60.58	62.68	65.59	68.33	72.14	77.91	84.24

(c) Target in-track percentage for a range of turn rates

Turn-Rate	1	1.5	2	2.5	3	3.5	4	4.5
All-CW	99.13	98.24	96.85	95.81	92.72	90.02	88.44	85.41
All-FM	94.68	91.98	91.03	89.91	88.93	87.88	86.51	84.70
PSBS	97.12	96.20	96.56	96.05	95.51	95.19	94.79	93.84

Turn-Rate	5	5.5	6	6.5	7	7.5	8	8.5
All-CW	82.89	78.97	77.05	73.77	70.97	65.81	58.77	53.23
All-FM	82.22	78.87	75.64	70.75	66.47	61.09	55.51	50.90
PSBS	92.97	91.90	90.48	87.12	84.37	78.96	69.20	61.47

Appendix B: EPSBS Performance Comparison Tables

In this appendix, the performance comparison tables, presenting the performance metrics, for the All-CW, All-FM, PSBS, and EPSBS approaches, for turn rates ranging from 1°/sec to 8.5°/sec and for measurement noise scenarios V_1 and V_2, are presented. The performance shown in the comparison tables is the averaged performance over 3000 Monte Carlo simulations. The data related to the figures 5.12 and 5.13 displayed in chapter 5 are presented in table B.1. Similarly, the data related to the figures 5.14 and 5.15 displayed in chapter 5 are presented in table B.2.

Each performance comparison table is subdivided into three sub-tables: (a), (b), and (c). Sub-table (a) presents a version of measurement noise, in terms of standard deviation (σ) of a zero-mean Gaussian noise in their corresponding dimensions, used in the generation of CW and FM versions of target-generated measurements in the measurement data. Sub-table (b) shows the averaged tracking filter performance, in terms of target position root mean square error, with All-CW, All-FM, PSBS, and EPSBS approaches, for turn-rates ranging from 1°/sec to 8.5°/sec. Sub-table (c) shows the averaged tracking filter performance, in terms of target in-track percentage, with All-CW, All-FM, PSBS, and EPSBS approaches, for turn-rates ranging from 1°/sec to 8.5°/sec.

Table B.1: EPSBS performance comparison table for measurement noise version V_1

(a) Measurement noise version V_1

	CW	FM
σ_{Range}	$40m$	$10m$
σ_{Bearing}	$1°$	$1°$
$\sigma_{\text{RangeRate}}$	$0.5m/sec$	-

(b) Target position root mean square error (in Meters) for a range of turn rates

Turn-Rate	1	1.5	2	2.5	3	3.5	4	4.5
All-CW	49.43	50.56	51.48	52.42	53.90	54.73	55.92	56.82
All-FM	45.67	46.18	46.97	48.31	50.01	51.17	52.65	53.88
PSBS	44.70	45.40	46.07	47.05	48.48	49.35	50.61	51.37
EPSBS	44.69	45.39	46.09	47.04	48.40	49.31	50.57	51.24

Turn-Rate	5	5.5	6	6.5	7	7.5	8	8.5
All-CW	57.81	59.45	60.73	61.30	62.99	64.57	66.04	67.95
All-FM	55.41	57.75	59.47	62.18	65.65	68.93	72.83	76.35
PSBS	52.31	53.84	55.11	56.28	58.25	59.85	62.60	64.83
EPSBS	52.16	53.63	54.81	55.64	57.47	58.91	60.96	62.82

(c) Target in-track percentage for a range of turn rates

Turn-Rate	1	1.5	2	2.5	3	3.5	4	4.5
All-CW	99.57	99.17	98.80	98.36	98.02	97.54	96.72	96.19
All-FM	97.49	96.93	96.77	96.26	95.84	95.98	95.41	95.36
PSBS	97.84	97.20	97.42	97.38	97.31	97.76	97.62	97.78
EPSBS	97.83	97.14	97.39	97.34	97.46	97.77	97.64	98.01

Turn-Rate	5	5.5	6	6.5	7	7.5	8	8.5
All-CW	95.42	94.89	93.48	93.51	92.44	90.96	90.28	87.21
All-FM	94.58	93.32	92.30	90.00	86.57	83.29	79.42	74.36
PSBS	97.94	97.65	96.81	96.39	95.04	93.79	91.67	89.07
EPSBS	98.04	97.90	97.27	97.14	96.30	95.48	93.90	92.29

Table B.2: EPSBS performance comparison table for measurement noise version V_2

(a) Measurement noise version V_2

	CW	FM
$\boldsymbol{\sigma}_{\text{Range}}$	75m	25m
$\boldsymbol{\sigma}_{\text{Bearing}}$	1°	1°
$\boldsymbol{\sigma}_{\text{RangeRate}}$	0.5m/sec	-

(b) Target psotion root mean square error (in Meters) for a range of turn rates

Turn-Rate	1	1.5	2	2.5	3	3.5	4	4.5
All-CW	53.89	54.40	55.61	56.60	58.24	60.61	62.40	64.39
All-FM	52.80	53.97	55.89	57.46	59.54	61.73	64.11	66.46
PSBS	48.56	49.21	50.19	51.28	52.72	54.14	55.64	57.04
EPSBS	48.59	49.25	50.21	51.28	52.73	54.04	55.62	57.04

Turn-Rate	5	5.5	6	6.5	7	7.5	8	8.5
All-CW	66.67	69.91	72.87	75.66	78.17	81.35	85.22	90.36
All-FM	68.98	72.69	76.81	80.99	85.23	89.27	92.95	97.45
PSBS	58.32	60.58	62.68	65.59	68.33	72.14	77.91	84.24
EPSBS	58.06	60.26	61.95	64.48	67.07	69.90	75.00	80.66

(c) Target in-track percentage for a range of turn rates

Turn-Rate	1	1.5	2	2.5	3	3.5	4	4.5
All-CW	99.13	98.24	96.85	95.81	92.72	90.02	88.44	85.41
All-FM	94.68	91.98	91.03	89.91	88.93	87.88	86.51	84.70
PSBS	97.12	96.20	96.56	96.05	95.51	95.19	94.79	93.84
EPSBS	97.07	96.10	96.46	95.81	95.27	95.03	94.34	93.22

Turn-Rate	5	5.5	6	6.5	7	7.5	8	8.5
All-CW	82.89	78.97	77.05	73.77	70.97	65.81	58.77	53.23
All-FM	82.22	78.87	75.64	70.75	66.47	61.09	55.51	50.90
PSBS	92.97	91.90	90.48	87.12	84.37	78.96	69.20	61.47
EPSBS	92.58	90.89	90.05	87.32	84.09	80.56	71.89	64.55

Appendix C: Matlab Code for Project Implementation

We used MATLAB software for project implementation and conducting Monte Carlo simulations. The m-files developed as a part of the project are made publicly available on a Github repository with a link as follows:

`https://github.com/venkatasasikiran/UKFPDAF-predictAhead2.git`

Bibliography

[1] X. Lurton, *An introduction to underwater acoustics: principles and applications.* springer, 2002.

[2] R. O. Nielsen, *Sonar signal processing.* Artech House, Inc., 1991.

[3] R. E. Hansen, "Introduction to sonar," *Course Material to INF-GEO4310, University of Oslo,(Oct. 7, 2009)*, 2009.

[4] R. P. Hodges, *Underwater Acoustics: Analysis, Design and Performance of Sonar.* Wiley, 2010.

[5] A. D. Waite and A. Waite, *Sonar for practising engineers.* Wiley London, 2002, vol. 3.

[6] T. Collins, "Active sonar pulse design." Ph.D. dissertation, University of Birmingham, 1996.

[7] A. A. Winder, "Ii. sonar system technology," *IEEE Transactions on Sonics and Ultrasonics*, vol. 22, no. 5, pp. 291–332, 1975.

[8] R. J. Urick, *Principles of underwater sound for engineers.* Tata McGraw-Hill Education, 1967.

[9] J. H. Steele, K. K. Turekian, and S. A. Thorpe, *Encyclopedia of ocean sciences*, 2010, p. 323.

[10] M. Ainslie, *Principles of Sonar Performance Modelling (Springer Praxis Books).* Springer, 2010.

[11] V. V. Kadam and R. Nayak, "Basics of acoustic science," in *Acoustic Textiles.* Springer, 2016, pp. 33–42.

[12] J.-P. Marage and Y. Mori, *Sonar and Underwater Acoustics.* Wiley-ISTE, 2010.

[13] A. Baldacci and G. Haralabus, "Signal processing for an active sonar system suitable for advanced sensor technology applications and environmental adaptation schemes," in *2006 14th European Signal Processing Conference.* IEEE, 2006, pp. 1–5.

[14] X. R. Li and V. P. Jilkov, "Survey of maneuvering target tracking: dynamic models," in *Signal and Data Processing of Small Targets 2000*, vol. 4048. International Society for Optics and Photonics, 2000, pp. 212–236.

[15] Y. Bar-Shalom, P. K. Willett, and X. Tian, *Tracking and Data Fusion: A Handbook of Algorithms.* Yaakov Bar-Shalom, 2011.

[16] M. Athans and F. C. Schweppe, "Optimal waveform design via control theoretic concepts," *Information and Control*, vol. 10, no. 4, pp. 335–377, 1967.

[17] D. J. Kershaw and R. J. Evans, "Optimal waveform selection for tracking systems," *IEEE Transactions on Information Theory*, vol. 40, no. 5, pp. 1536–1550, 1994.

[18] ——, "Waveform selective probabilistic data association," *IEEE Transactions on Aerospace and Electronic Systems*, vol. 33, no. 4, pp. 1180–1188, 1997.

[19] S. P. Sira, A. Papandreou-Suppappola, and D. Morrell, "Dynamic configuration of time-varying waveforms for agile sensing and tracking in clutter," *IEEE Transactions on Signal Processing*, vol. 55, no. 7, pp. 3207–3217, 2007.

[20] C. Rago, P. Willett, and Y. Bar-Shalom, "Detection-tracking performance with combined waveforms," *IEEE Transactions on Aerospace and Electronic Systems*, vol. 34, no. 2, pp. 612–624, 1998.

[21] S. Yan, P. Willett, and R. Lynch, "Waveform fusion for sonar detection and estimation," in *Acoustics, Speech, and Signal Processing (ICASSP), 2002 IEEE International Conference on*, vol. 3. IEEE, 2002, pp. III–2973.

[22] S. Haykin, "Cognitive radar: a way of the future," *IEEE signal processing magazine*, vol. 23, no. 1, pp. 30–40, 2006.

[23] G. T. Capraro, A. Farina, H. Griffiths, and M. C. Wicks, "Knowledge-based radar signal and data processing: a tutorial review," *IEEE Signal Processing Magazine*, vol. 23, no. 1, pp. 18–29, 2006.

[24] J. R. Guerci, "Cognitive radar: A knowledge-aided fully adaptive approach," in *2010 IEEE Radar Conference*. IEEE, 2010, pp. 1365–1370.

[25] S. Haykin, Y. Xue, and P. Setoodeh, "Cognitive radar: Step toward bridging the gap between neuroscience and engineering," *Proceedings of the IEEE*, vol. 100, no. 11, pp. 3102–3130, 2012.

[26] J. M. Fuster, *Cortex and mind: Unifying cognition.* Oxford university press, 2003.

[27] K. L. Bell, C. J. Baker, G. E. Smith, J. T. Johnson, and M. Rangaswamy, "Cognitive radar framework for target detection and tracking," *IEEE Journal of Selected Topics in Signal Processing*, vol. 9, no. 8, pp. 1427–1439, 2015.

[28] A. Charlish and F. Hoffmann, "Anticipation in cognitive radar using stochastic control," in *2015 IEEE Radar Conference (RadarCon)*. IEEE, 2015, pp. 1692–1697.

[29] W. Li, G. Chen, E. Blasch, and R. Lynch, "Cognitive mimo sonar based robust target detection for harbor and maritime surveillance applications," in *2009 IEEE Aerospace conference*. IEEE, 2009, pp. 1–9.

[30] L. Xiaohua, L. Yaan, L. Guancheng, and Y. Jing, "Research of the principle of cognitive sonar and beamforming simulation analysis," in *2011 IEEE International Conference on Signal Processing, Communications and Computing (ICSPCC)*. IEEE, 2011, pp. 1–5.

[31] X. Li, Y. Li, L. Cui, and W. Liu, "Research of new concept sonar-cognitive sonar," *Journal of Marine Science and Application*, vol. 10, no. 4, pp. 502–509, 2011.

[32] T. Claussen and V. D. Nguyen, "Real-time cognitive sonar system with target-optimized adaptive signal processing through multi-layer data fusion," in *2015 IEEE International Conference on Multisensor Fusion and Integration for Intelligent Systems (MFI)*. IEEE, 2015, pp. 357–361.

[33] S. Schoenecker *et al.*, "Goal driven autonomy as a model for reasoning in cognitive active sonar," in *2018 IEEE 10th Sensor Array and Multichannel Signal Processing Workshop (SAM)*. IEEE, 2018, pp. 1–5.

[34] Y. Bar-Shalom, X. Li, T. Kirubarajan, and J. Wiley, "Estimation for kinematic models," in *Estimation with applications to tracking and navigation*. Wiley Online Library, 2001.

[35] S. J. Julier, J. K. Uhlmann, and H. F. Durrant-Whyte, "A new approach for filtering nonlinear systems," in *American Control Conference, Proceedings of the 1995*, vol. 3. IEEE, 1995, pp. 1628–1632.

[36] M. S. Grewal and A. P. Andrews, *Kalman Filtering: Theory and Practice with MAT-LAB (Wiley - IEEE)*. Wiley-IEEE Press, 2014.

Curriculum Vitae

Venkata Sasikiran Veeramachaneni is a Master of Science student in the Department of Electrical and Computer Engineering (ECE) at George Mason University. He received the Bachelor of Technology degree in Electrical and Electronics Engineering from Jawaharlal Nehru Technological University Kakinada, India in 2014. From July 2014 to July 2015, he worked at Tata Consultancy Services Ltd, Hyderabad, India as an Assistant System Engineer. In Fall-2015, he started his master's degree in Electrical Engineering major with a focus in Controls and Robotics. He worked as a Graduate Teaching Assistant with the ECE department for Spring-2016 and Fall-2016 semesters. From January 2017 until the present, he has been working as a Graduate Research Assistant with Ocean Acoustics and Signal Processing lab. He received the ECE department's Outstanding Academic Achievement award for 2018. His primary interests are Control Systems, Signal Processing, Machine learning, Artificial Intelligence, and Robotics.